energies

MDPI

Review

Shear Wave Velocity Applications in Geomechanics with Focus on Risk Assessment in Carbon Capture and Storage Projects

Mitra Khalilidermani and Dariusz Knez *

Department of Drilling and Geoengineering, Faculty of Drilling, Oil, and Gas, AGH University of Krakow, 30-059 Krakow, Poland; mitra@agh.edu.pl

* Correspondence: knez@agh.edu.pl; Tel./Fax: +48-12-617-3784

Abstract: Shear wave velocity (Vs) has significant applications in geoengineering investigations. With the ongoing rise in carbon capture and storage (CCS) initiatives, the role of Vs in monitoring the CO_2 sequestration sites is escalating. Although many studies have been conducted to assess CCS-induced risks, no inclusive research has been conducted integrating those investigations. This study strives to collate and integrate the applications of Vs in geoscience with an emphasis on CCS risk assessment. Based on this research, major CCS-induced risks were detected: induced seismicity, caprock failure, groundwater contamination, fault reactivation, and reservoir deformation. These risks were inclusively described, and the mathematical formulations incorporating the Vs parameter in risk analysis were elaborated. It was concluded that Vs applications can be further extended in monitoring CO_2 plume migration, optimizing CO_2 injection pressures, preventing shallow water contamination, and predicting CCS-induced seismic events. All these applications require fully coupled hydromechanical analysis based on poroelasticity theory. Hence, various factors including pore pressure, in situ stresses, faults distribution, and poroelastic parameters must be carefully determined before the CO_2 injection phase. The mathematical formulations presented in the present study are quite applicable for granting the safety and long-term success of subsurface carbon sequestration.

Keywords: CCS; underground storage; risk assessment; seismic exploration; wave propagation; geomechanics; poroelasticity

Citation: Khalilidermani, M.; Knez, D. Shear Wave Velocity Applications in Geomechanics with Focus on Risk Assessment in Carbon Capture and Storage Projects. *Energies* **2024**, *17*, 1578. https://doi.org/10.3390/en17071578

Academic Editors: Maris Klavins and Linda Ansone-Bertina

Received: 27 February 2024
Revised: 21 March 2024
Accepted: 23 March 2024
Published: 26 March 2024

1. Introduction

Measuring the speed of sonic waves traveling within a rock results in an index known as velocity. In the case of an isotropic, homogeneous, and linearly elastic rock, only two acoustic wave types can propagate: compressional waves and shear waves. Typically, the velocity of compressional waves is approximately double that of shear waves within rocks. In geomechanics, Vs is applied mainly to ascertain the stiffness and mechanical features of subsurface rocks [1]. In fact, it helps in gaining a deeper comprehension of the behavior of rocks, soils, and sediments under various geological and geotechnical conditions [2].

Vs is fundamentally pertinent to the elastic properties of subsurface formations. In an isotropic elastic rock, the magnitude of Vs can be calculated as [3]:

$$V_S = \sqrt{\frac{G}{\rho}} \quad (1)$$

In the above equation, Vs depicts the velocity of the shear wave (m/s), G indicates the rock's shear modulus (Pa), and ρ represents the rock's density (kg/m^3). The provided equation illustrates a direct proportionality between Vs and the square root of the shear modulus. Conversely, Vs demonstrates an inverse correlation with the square root of the rock's density.

The Vs may be directly estimated through laboratory tests as well as on-site surveys. Regarding the laboratory tests, the acoustic waves are propagated through small-sized rock specimens by acoustic wave propagation apparatus [4]. Then, the parameters of Vs and compressional wave velocity (Vp) are recorded. On the contrary, in the field, the Vs can be measured through borehole measurements, Dipole shear sonic imagers (DSIs), and geophysical techniques [5].

In recent decades, applications of Vs data in geoengineering projects have significantly increased. In fact, in the past, Vs measurements have mainly been applied in earthquake engineering [5], geotechnical site characterization [6,7], oil and gas reservoir exploration [8], and aquifer assessments [9]. However, nowadays, it is being used in geothermal resources detection [10], landslide potential analysis [11], geohazard evaluation of seabed formations [12], deep Earth exploration [13], and CCS projects [14].

Climate change has emerged as a shared global challenge. The escalation of industrial activities to meet the growing needs of the expanding global population is contributing to a continuous rise in greenhouse gas emissions and the Earth's temperature [15]. The warmest year on record, which was previously 2016, is now 2023 [16]. According to ERA5, which stands for the "Fifth Generation of the European Centre for Medium-Range Weather Forecasts (ECMWF) Reanalysis", the global average temperature in 2023 was 14.98 °C, indicating a 0.17 °C rise compared to the measurements recorded in 2016 [16].

Over the past few decades, the release of greenhouse gases has led to rising temperatures, increased sea levels, and intense climate consequences [17,18]. Human-generated emissions have resulted in global warming of 1.0 °C. Carbon dioxide gas stands out as the most significant contributor, accounting for approximately 72% of the current global warming effects [19]. Figure 1 depicts the increase in global temperature derived from anthropogenic CO_2 emissions [19]. Based on this figure, during 2030–2052, the earth will reach a 1.5 °C increase in temperature. This rise in temperature contributes to rising sea levels, and to the occurrence of harsh climate consequences such as heatwaves, heavy rainfall, hurricanes, droughts, and storms [15]. The exponential trajectory of anthropogenic warming is anticipated to reach 2 °C by the year 2060 [19].

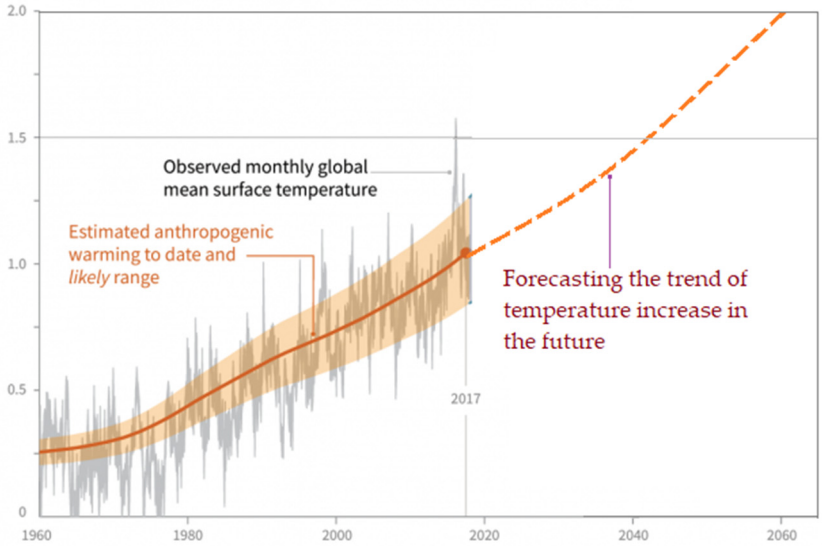

Figure 1. The effect of human-generated emissions on the global temperature increase [19].

Offering an effective approach to mitigating greenhouse gases, CCS technology directly contributes to the objective of carbon reduction [20]. The CO_2 generated by stationary sources, primarily from industrial facilities such as power plants, undergoes initial collection and liquefaction. The liquefied carbon dioxide is then injected to subsurface porous rocks [21]. During this stage, a substantial volume of supercritical CO_2 is injected into underground storage. Geologically, the CO_2 injection process disrupts the local stress regime, potentially posing environmental risks in the region [22].

The major environmental risks of CCS projects are induced seismicity [23,24], caprock failure [25,26], groundwater contamination [27,28], fault reactivation [29,30], and reservoir deformation [31]. The extent of those environmental risks depends mainly on the on-site geology, the local tectonics regime, the caprock sealing capacity, the volume of the injected CO_2, the storage depths, etc. [21]. The larger extent of those risks, the higher the potential for CO_2 leakage, seismic events, groundwater contamination, reservoir damage, etc.

Vs data are applicable for site selection in CCS projects; also, they can be utilized for monitoring the carbon dioxide plume within the storage formation and behind [32–36]. In fact, by comparing Vs profiles before and after CO_2 injection, the changes in the rock's saturation degree, the rocks' elasticity modules, the local faults stability, the groundwater flow regime, etc., can be evaluated [32]. So far, many investigations have assessed the CCS-induced environmental risks in different projects [37–40]. In Section 3, an overall description of those investigations, together with their key findings, have been presented.

The key aim of the current study is to impart an up-to-date status of advancements in shear wave velocity applications in geomechanics, with emphasis on CCS projects. As a matter of fact, those ongoing advancements are continuing to progress, with more applications emerging to deal with fluid injection and production from underground. Therefore, this research strives to collate the findings of previous investigations and elaborate upon the most applicable aspects of shear wave velocity in risk assessments of CCS projects. Moreover, the analytical theories and mathematical formulations essential for addressing each CCS-induced risk are described individually. The authors conceive that this research provides an up-to-date source focusing on the risk assessment of CCS projects from a geomechanics viewpoint.

This study is structured as follows: Initially, Section 2 describes the major conventional and emerging utilizations of the Vs parameter in geomechanics. Then, in Section 3, CCS technology, along with the global dispersion of large CCS projects, are presented. Afterward, the different types of geological formations that are suitable for CO_2 sequestration are recounted. Subsequently, the major CCS-induced risks, together with their solutions in the form of mathematical formulations, are elaborated. Then, the most significant findings of the research are discussed in the Discussion. And, in the final section, the paper wraps up with the Conclusion, presenting the key results, future recommendations, and potential implications.

2. Applications of the Vs Parameter in Geomechanics

Vs is utilized in an extensive range of geomechanics applications. In general, those applications can be broken down into two primary categories: conventional and emerging. Figure 2 illustrates those applications. They are elaborated upon in the subsequent sections. The application of Vs data in CCS projects is comprehensively described in Section 3.

2.1. Conventional Applications

2.1.1. Earthquake Engineering

Vs holds an essential role in assessing the hazards that stem from earthquakes [5]. It helps in predicting the dynamic behaviors of soils and rocks during earthquakes. Researchers have conducted studies to investigate the correlation between Vs and ground motion amplification [41]. Boore et al. investigated the relation between Vs and ground motion amplification in the San Francisco Bay region [41]. Empirical relationships were proposed to correlate Vs with the peak ground acceleration (PGA) parameter.

Vs can also be applied in the estimation of the dynamic characteristics of soils and rocks, e.g., shear modulus, which influence the response of the ground during earthquakes. Dong et al. developed a correlation between Vs and soils' shear moduli [42]. Vs is also employed in seismic site classification to categorize the different regions based on their geological and geotechnical properties [43,44]. An example of such research includes the work by Idriss and Boulanger, which proposed a site classification system for seismic design in California [45].

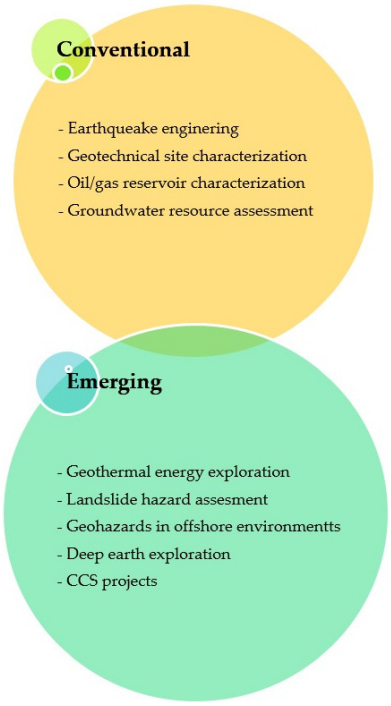

Figure 2. The conventional and emerging applications of shear wave velocity in geoscience.

2.1.2. Geotechnical Site Characterization

Shear wave velocity is also extensively applied in geotechnical site characterization, especially in the assessment of the mechanical properties and behaviors of subsurface soils/rocks [6,7,46]. For instance, it is used to assess the soils' strength properties, which are crucial for foundation design, slope stability, and ground improvement projects. Researchers have conducted studies to evaluate the correlation between the Vs and soil strength properties like shear modulus and Young's modulus. As an example, Uma Maheswari et al. developed some empirical relations between Vs and soil properties to estimate the shear strength of soils [47]. In another study, Oh et al. studied the relationship between Vs and the undrained shear strength of clays for structure designs [48]. Vs also helps to evaluate the liquefaction potential of soils during earthquakes [49]. For instance, Yunmin et al. conducted studies correlating Vs with the liquefaction risk of various soil types [50].

2.1.3. Reservoir Characterization

The Vs is an essential parameter in reservoir characterization, particularly in estimating the mechanical properties of rocks [51]. It is also used to identify lithological variations within the reservoirs since different rock types exhibit distinct Vs values due to variations in their mineralogy, porosity, and diagenesis. Wang et al. utilized the Vs data to detect the reservoir lithology in the Tarim Basin, China [52].

Moreover, Vs data are employed for the estimation of rocks' porosity. For instance, Kováčik and Emmer investigated the empirical equations correlating Vs with rock porosity in some sedimentary formations [53]. Furthermore, shear wave velocity can be utilized to evaluate fluid content within reservoirs. In fact, pore fluids, e.g., oil, gas, and brine, influence the shear wave velocity of the reservoir formations. As an example, Korneev proposed a method to estimate fluid saturation from Vs data [54].

2.1.4. Groundwater Resource Assessment

Shear wave velocity data also provide valuable information about aquifers' characteristics [9]. They aid in assessing various properties, like hydraulic conductivity, permeability, storativity, and porosity. For example, Azhar et al. conducted a study correlating Vs with groundwater potential in the coastal aquifer in Brunei Darussalam [55]. Vs profiles can

be also used to simulate the groundwater flow in aquifers [56]. In addition, a number of researchers have employed Vs data to assess the potential of seawater intrusion into coastal aquifers [57]. This application originates from the fact that the presence of saline water affects the Vs of groundwater-bearing formations. For instance, Alhumimidi proposed a method applying Vs to identify seawater intrusion in Saudi Arabia [57]. Additionally, Vs measurements can be applied in creating groundwater resource maps. An example includes the work by Mourad et al., who employed Vs data to map the aquifer potential in the Kumamoto region in Japan [58].

2.2. Emerging Applications

Vs prediction continues to find new applications in various areas of geoscience. Some emerging utilizations of Vs parameter are presented in the following subsections.

2.2.1. Geothermal Energy Exploration

Vs surveys are an indispensable aspect of reservoir characterization for geothermal energy exploration. Vs prediction helps in identifying favorable reservoir zones, estimating their permeability and porosity, and optimizing the placement of geothermal injection and production wells [59]. Furthermore, Vs data can assist in detecting and assessing the fractures and fault zones within geothermal reservoirs. In a research project, Lou and Rial used Vs data to characterize fractures and cracks in geothermal reservoirs in California, USA [60]. Vs profiles are also applicable in mapping geothermal resources. By estimating Vs, researchers can assess the subsurface heat transfer and identify areas with high geothermal gradients. Vs prediction aids in evaluating the thermal conductivity and heat storage capacity of rocks, assisting in the identification of appropriate locations for geothermal power generation [61]. It is noteworthy that Vs data are also beneficial in designing enhanced geothermal systems (EGS). As a matter of fact, they help in optimizing hydraulic fracturing designs, estimating permeability enhancement, and monitoring reservoir responses during stimulations [62].

2.2.2. Landslide Hazard Assessment

Vs measurements can be employed in the prediction of landslide events [63]. By estimating Vs, areas with low shear wave velocities can be detected, indicating potential weak zones that are susceptible to landslides. Consequently, the appropriate slope stabilization measures can be taken. One reference to this application is the study carried out by Qureshi et al., who utilized Vs data to evaluate the onset of landslide hazards in Japan and Pakistan [64]. Furthermore, Vs data can be applied in developing early-warning systems for landslide prediction [65]. For instance, Chen et al. used Vs measurements and monitoring data to establish a preemptive alert system for landslides occurrence caused by intense rainfall in China [65]. Another application of Vs is to assess the propagation of seismic waves derived from landslides and evaluate their potential impact on nearby structures [66].

2.2.3. Geohazard Assessment in Offshore Environments

Vs data can also be used in the evaluation of seabed stability in offshore environments. By measuring Vs, engineers can evaluate the strength properties of seabed sediments, helping to identify regions prone to submarine landslides. Consequently, the design and placement of offshore infrastructure are optimized [67]. In a research project, Ten Brink et al. incorporated Vs in an assessment of potential submarine landslide hazards on the eastern coast of the USA [68]. Moreover, Vs data can be employed in the designation of offshore infrastructure, such as oil and gas platforms, subsea pipelines, and renewable energy installations. In fact, Vs data provide engineers with information of soil stiffness and dynamic behavior of the seabed, assisting them in the design of stable offshore foundations [69]. In a research project, Huijer et al. utilized Vs and other seismic data to assess potential seismic hazards in the south of Lebanon [70].

2.2.4. Deep Earth Exploration

Vs data measured from Earth's deep interior provide invaluable information about our planet [71]. They help in revealing complex processes, such as plate tectonics and mantle convection. Furthermore, seismic measurements pertinent to Earth's core help geoscientists in better understanding phenomena such as Earth's magnetism and core dynamics. In an interesting study, Gao et al. utilized compressional and shear wave tomography data to study the mantle convection process in the central Rio Grande rift in the USA [72]. In a recent investigation, Zhang et al. deployed Vs data obtained from the upper mantle and Earth's crust for geodynamic applications and investigations into the fractures in Southeastern Tibet [73]. In another study, Butler and Tsuboi used shear wave velocity seismic surveys to study Earth's inner core [74].

3. Vs Applications in Risk Assessment of CCS Projects

This section begins with a concise description of supercritical CO_2 and CCS processes, and potential geological formations for CCS purposes. Afterward, the CCS-induced environmental risks are described.

3.1. Supercritical CO_2 and CCS Projects

CO_2 gas lacks odor and color, and it is denser than air. Moreover, its characteristics are contingent on pressure–temperature (P–T) circumstances. Under atmospheric temperature and pressure, it exists in the gaseous phase. When subjected to low temperatures (under 78°C), carbon dioxide transforms into a solid [39]. At temperatures between 56.5 and 31.1°C, CO_2 exists as a gas. However, when temperatures exceed 31.1°C and pressures exceed 7380 kPa, it transitions into a supercritical phase [39]. This feature is of paramount significance for CCS operations as carbon dioxide must be injected in supercritical form due to its higher density compared to the gaseous phase [75]. In a typical CO_2 sequestration reservoir, the temperature and pressure levels are commonly higher than those of a supercritical state of CO_2 [39].

CCS technologies are fundamentally perceived as potential tools for tackling the impact of fossil fuels on climate change. This involves taking CO_2 emissions produced by industrial plants and transporting the captured CO_2 to an underground storage site to store it [20]. The primary stages of sequestration operations have been depicted in Figure 3. Firstly, carbon dioxide is collected from production origins such as coal mining projects, gas fields, and industries with high-intensity CO_2 emissions like steel and cement manufacturing [21]. Then, after undergoing appropriate treatments, which may include pressurization, liquefaction, or hydrate formation, the captured CO_2 is transported to designated injection sites. And finally, the CO_2 is injected into underground geological formations [21]. CCS is considered to be a critical tool for reducing carbon emissions and climate change consequences. Figure 4 shows a global map of CCS projects, as of March 2022 [76].

3.2. Types of Underground Storage Sites

Supercritical CO_2 is injected mainly into underground structures encompassing deep-seated saline aquifers and exhausted hydrocarbon reservoirs [21]. Regarding the depleted hydrocarbon reservoirs, the CCS may be conducted for two purposes, including carbon sequestration and enhanced oil recovery (EOR) purposes. Except those two mentioned formations, the CO_2 can also be stored in coal seams, particularly for enhanced coal bed methane (CBM) initiatives [78,79]. However, this type of CO_2 sequestration is not remarkably prevalent.

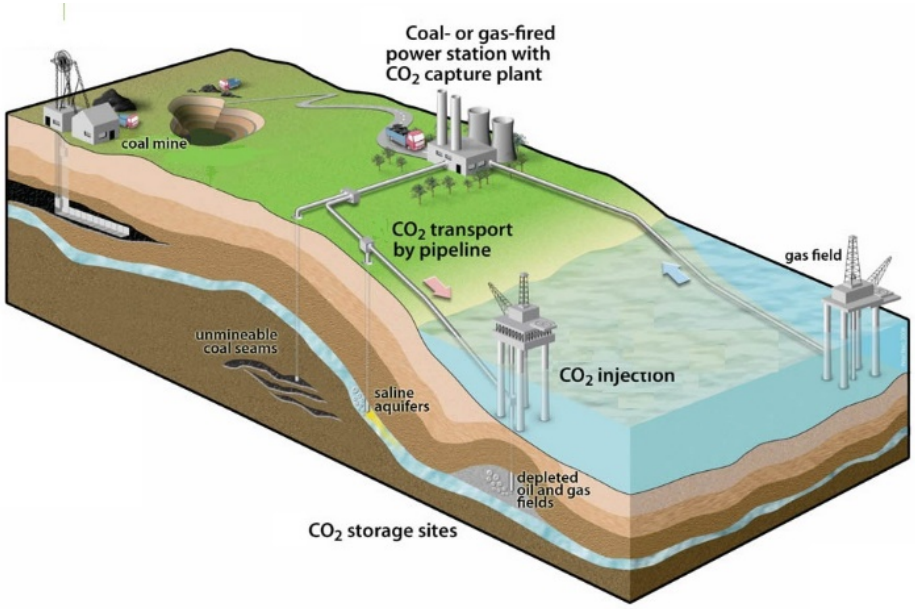

Figure 3. A schematic view of CCS process [76].

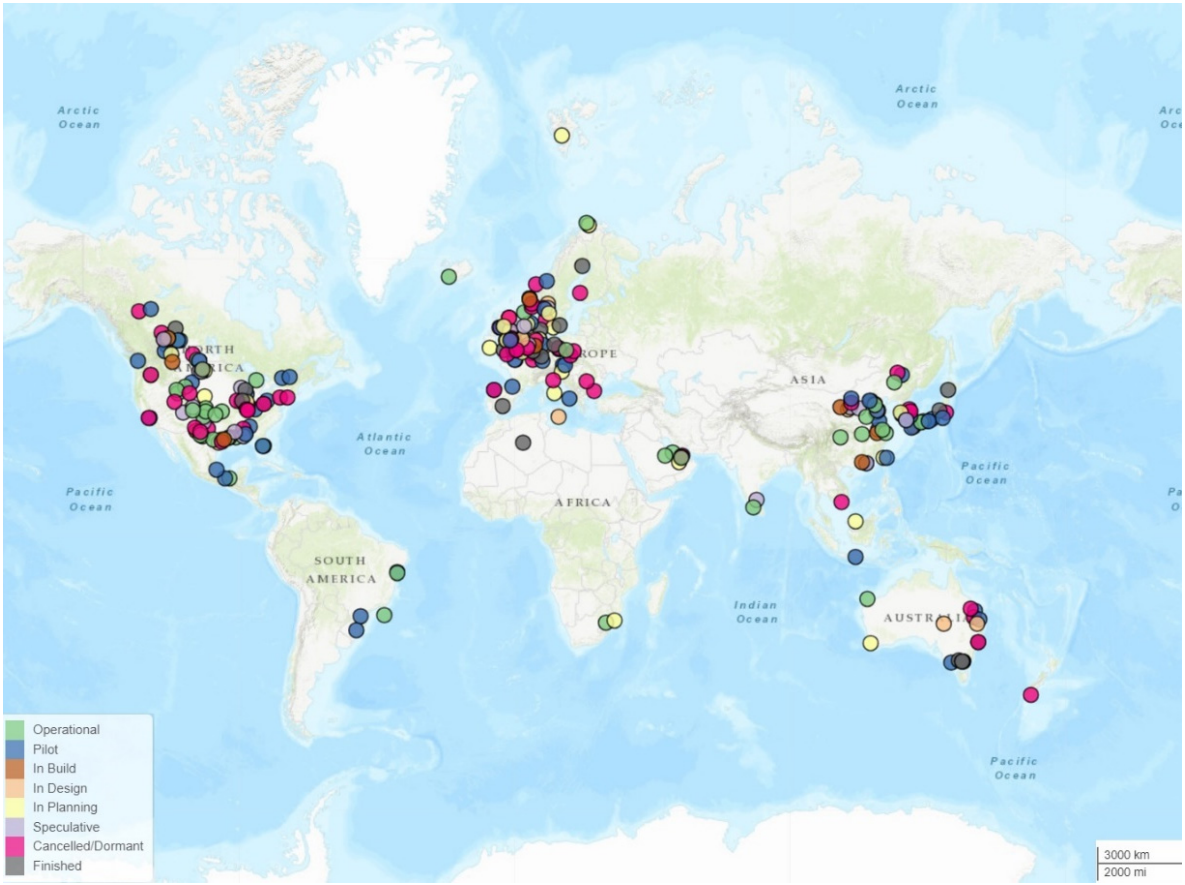

Figure 4. A global map of CCS projects executed as of March 2022 [77].

Figure 5 illustrates the relative potentials of different subsurface formations for CCS projects in the world [39]. As can be seen, the most frequent scenario for CCS storage is deep saline aquifers. Conversely, only 0.01% of the potential CCS operations are carried out in mineral sequestration. This technique involves capturing CO_2 emissions and converting them into stable carbonate minerals through a chemical reaction with certain minerals, contributing to long-term carbon storage [80].

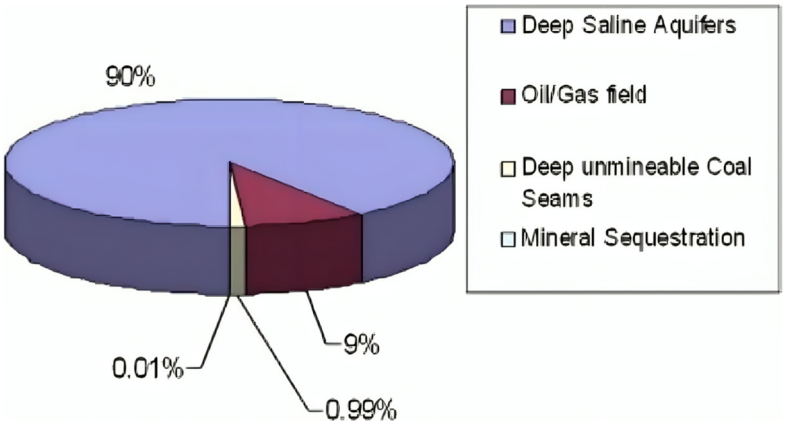

Figure 5. The relative potential of the implementation of CCS operations in different geological formations [39].

Ensuring the enduring storage of CO_2 is best achieved by selecting sites with substantial depth, usually exceeding 800 m. These sites should possess ample capacity and incorporate an effective sealing caprock to prevent the containment of groundwater resources [25,26]. So far, numerous experimental investigations have been undertaken to explore the carbon dioxide repercussions for the physical and mechanical features of hosting formations [81]. These investigations illustrated that the temporary effects for the mechanical properties of rocks are generally limited in many sedimentary reservoirs. However, carbonate reservoirs, which display a diverse range of responses, tend to experience more critical impacts. Table 1 outlines the sequestration prospects within the United States, along with the corresponding risk levels associated with each sequestration strategy [39].

Table 1. The degree of storage capacity, storage integrity, and environmental risks related to different geological formations for CCS purposes [39].

CCS Option	Storage Capacity ($Gt\text{-}CO_2$)	Storage Integrity	Environmental Risk
Depleted oil and gas fields	25–30	High	Low
Active oil wells (EOR)	Low	High	Low
Enhanced coal bed methane	5–10	Medium	Medium
Deep aquifers	1–150	Medium	Medium
Ocean (global)	1000–10,000	Medium	High
Carbonate storage (no transport)	Very high	Highest	High

Figure 6 illustrates a global map of CCS projects categorized on the basis of geological storage formations [77].

CCS operation in saline aquifers involves injecting CO_2 into deep underground porous rocks saturated with saline water [30]. Saline aquifers offer significant storage potential due to their vast abundance globally. The advantages include a large storage capacity, wide distribution, and a reduced likelihood of competing land uses. Additionally, saline aquifers are not generally used for other purposes, minimizing potential conflicts. Nevertheless, the possible challenges include the need for extensive site characterization to ensure geological integrity, and the potential for induced seismicity. The regulatory framework must address caprock failure problems and potential groundwater contaminations [82]. Some notable CCS projects conducted in deep saline rocks are the Sleipner site in Norway [83], the Otway site in Australia [84,85], the Aquistore site in Canada [86], the Ketzin site in Germany [34], and the Decatur site in the United States of America [23].

CCS implementation in exhausted hydrocarbon reservoirs encompasses the process of injecting captured CO_2 into subsurface formations that were previously exploited for hydrocarbons. These reservoirs offer several advantages, including proven geological stability, existing infrastructure from the oil and gas industry, and potential economic incentives through EOR [87]. Depleted reservoirs provide a ready-made solution for

large-scale storage, leveraging the expertise gained from decades of oil and gas extraction. However, limitations include the finite availability of suitable sites, potential leakage pathways, and the need for careful assessment of caprock integrity to inhibit the upward movement of carbon dioxide [88]. Some large CCS projects operated in former hydrocarbon fields include the Canadian location known as the Weyburn–Midale site [89], the Algerian site called In Salah [90], and the Norwegian site called Snøhvit [91].

Figure 6. A global map of CCS projects categorized based on storage formations [77].

Unexploitable coal seams offer an alternative formation for anthropogenic carbon dioxide sequestration [78]. The primary storage mechanism involves the adsorption of CO_2 onto micropore surfaces within the coal matrix, distinguishing it from the hydrodynamic trapping observed in either saline aquifers or reservoirs of oil and gas [79]. Hypothetically, carbon dioxide must remain within the coal, provided that the formation pressure surpasses the desorption threshold pressure. Researchers, such as Mahajan [78] and Krooss et al. [79], have documented the CO_2 sorption characteristics and rock skeleton swelling linked to CO_2 adsorption. In addition, coal seams present a medium for simultaneous CBM exploitation along with CO_2 storage. Injecting carbon dioxide into deep-stated, non-mineable coal beds can boost commercial methane production, as CO_2 adsorption stimulates methane desorption. This dual-purpose approach holds the potential to store substantial amounts of carbon dioxide while enhancing the productivity of CBM activities. Some examples of CCS projects implemented in coal seams include the CO_2-CRC Otway Project in Australia [92], the Surat Basin CCS Project in Australia [93], and the Qinhuangdao Integrated CCUS Project in China [94].

3.3. Vs Applications in CCS-Induced Risk Assessment

Although CCS projects reduce greenhouse gas emissions, they may lead to some geomechanical and environmental risks [23–30]. Figure 7 shows the common concerns that arise in CCS projects: induced seismicity, caprock failure, groundwater contamination, fault reactivation, and reservoir deformation.

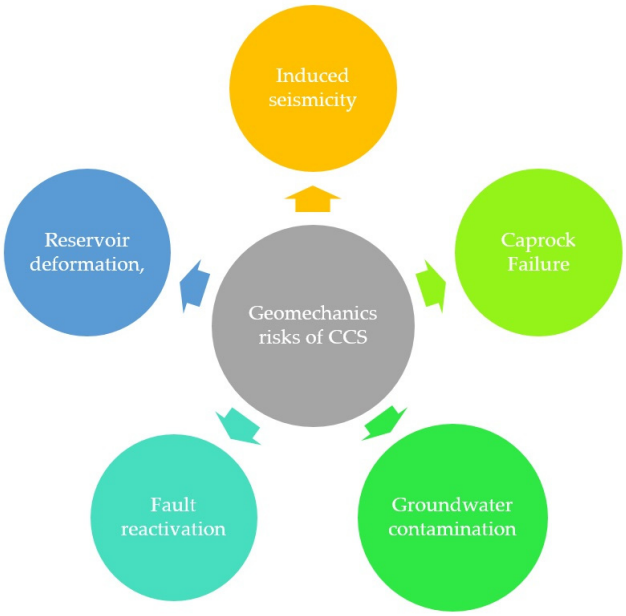

Figure 7. Common geomechanics concerns related to CCS projects.

By evaluating Vs profiles, one can discern critical information about the jeopardy of induced seismicity, the integrity of caprocks, the presence of faults, the potential for CO_2 leakage pathways, the extent of water contamination, and the mechanical stability of reservoirs. Table 2 summarizes the key applications of shear wave velocity in addressing the aforesaid CCS risks.

Table 2. Key applications of shear wave velocity in prediction and mitigation of CCS-derived risks.

Risk	Vs Application	Description
Induced seismicity	Seismic hazard assessment	Vs contributes to seismic hazard analysis, helping to model seismic wave propagation and scrutinize the possible impact of seismic events on the CCS projects and their adjacent structures.
	Site-specific seismic design	Shear wave velocity data inform site-specific seismic design considerations, allowing for the development of adjacent structures that can withstand the dynamic forces associated with seismic events.
Caprock failure	Assessment of sealing capacity and stability of caprock	Evaluation of Vs profiles helps in assessing the mechanical stability and integrity of caprocks; this is crucial for preventing CO_2 leakage and shallow groundwater containment.
Groundwater contamination	Mapping subsurface heterogeneity	Vs profiles provide insights into subsurface heterogeneity, allowing for the identification of anomalous zones and areas of structural weaknesses that may pose risks to groundwater containment (CO_2 intrusion).
Fault reactivation	Identification of faults and fractures	Vs data are used to detect and characterize faults and fractures within the subsurface, aiding in the assessment of potential pathways for CO_2 leakage.
Reservoir deformation	Monitoring changes over time	Continuous monitoring of shear wave velocity helps in tracking changes in subsurface conditions, enabling the early detection of potential risks such as caprock degradation, reservoir deformation, or CO_2 migration.
	Pore pressure assessment	Changes in shear wave velocity are indicative of variations in fluid content, aiding in the assessment of pore pressure changes that could influence the mechanical behavior of the storage reservoir.

3.3.1. Induced Seismicity Risk

Description

While CCS technology is an efficient approach for curbing CO_2 release into the atmosphere, the seismic activity resulting from CO_2 injection poses a substantial risk [84,86]. This seismicity not only represents a serious hazard but also acts as a hindrance to the progress of CO_2 geological storage. The potential risks associated with induced seismicity encompass several aspects. Firstly, the likely earthquakes or shakings could lead to casualties. Secondly, there is a risk of damage to infrastructure, particularly in cases where the CCS project is in close proximity to city areas. And thirdly, induced seismicity might compromise the integrity of caprocks, potentially cracking them, and allowing CO_2 to move towards the upper formations through the fractured zone [20,89].

Up to the present, numerous projects involving CO_2 injection have actively monitored induced seismic events [23]. Table 3 summarizes some of those major investigations. As can be seen, the majority of recorded seismic events were microseismic activities with magnitudes of less than 3 (i.e., $M < 3$). Moreover, in some cases, the magnitude has a negative value. It is worth mentioning that the magnitude of seismic events is generally a positive value, and it is not common to see negative values for earthquake magnitudes. However, there are instances where seismic events with magnitudes less than 0 can be reported. This may occur with microseisms or very small events that are detectable by seismographs, but which do not represent significant ground shaking. In other words, negative magnitudes are used to describe such small seismic events that fall below the detection threshold of larger earthquakes.

Generally, the reservoir's geological conditions, the local faults distribution regime, and the volume of the injected CO_2 influence the frequency and severity of CCS-induced seismicity. Thus, as can be seen in Table 3, the quantity and scale of reported seismic occurrences, triggered by human activities, were different in CCS projects [95]. Based on this table, the maximum magnitude of recorded seismic events was 4.4, which occurred in the Cogdell CCS project in the USA [95]. On the other hand, no induced seismic events were recorded in some CCS projects, such as Cranfield [96] and Aquistore [86].

Table 3. Major investigations pertinent to induced seismicity at CCS projects.

Project Name	Country	Storage Type	CO_2 Injected Volume/Tonnage	Number of Seismic Events	Seismic Magnitude	Detail of Seismic Events	Reference
Cogdell	United States	Oil reservoir (EOR)	85 million m^3 (per month)	18 1	$M \geq 3$ 4.4	The maximum seismic magnitude has been recorded in this project.	[95]
In Salah	Algeria	Oil reservoir (EOR)	4 million tons	>6000	$-1 \leq M \leq 1.7$	The seismic events were recorded by installments of monitoring sensors in three injection wells.	[20,97]
Decatur	United States	Deep saline reservoir	1 million tons	>10000	$-2 \leq M \leq 1$	As the injection duration increased, the spatial extent of the induced seismic activity also grew.	[23]
Aneth	United States	Oil reservoir (EOR)	694,449 tons	3800	$-1.2 \leq M \leq 0.8$	The seismic events were distributed around two faults 4.8 km far from the injection wells.	[23]
Lacq-Rousse	France	Depleted gas reservoir	>50,000 tons	600	$-2.3 \leq M \leq -0.5$	Near-surface and down-hole monitoring systems were used to record the seismic events.	[98]
Weyburn	Canada	Oil reservoir (EOR)	5.3 million tons (per year)	200	$-3 \leq M \leq -1$	The installation of a seismic monitoring system took place in an abandoned production oil well.	[20,23,89]
Otwey Basin	Australia	Oil reservoir (EOR)	65,445 tons	<5 events per day	$0 > M$	Injection of a supercritical fluid containing CO_2 and CH_4 into an underground reservoir at a depth reaching 2000 m.	[84,99]
Cranfield	United States	Deep saline aquifer	5 million tons	0	-	No induced seismicity was reported.	[96]
Aquistore	Canada	Deep saline aquifer	140,000 tons	0	-	No induced seismic event was recorded.	[86]

Formulations

Vs parameters can be utilized in different theories related to predicting CCS-induced seismic events. For instance, they can be incorporated in Biot's incremental theory, which is applied in the analysis of seismicity induced by fluid injection into underground formations [100,101]. This theory was developed by Kisslinger and Chery in 1970 [100]. They

demonstrated that, if a shear wave propagates through an area of active shear stress, the shear wave generates particle accelerations parallel to its direction. When the cumulative pressure from injection, along with tectonic stress, surpasses the inherent strength of the rock, it fractures, thereby initiating induced seismicity. According to this theory, the mechanism of triggering seismicity adheres to the effective stress theory as well as the Mohr–Coulomb rock failure criterion. They established fundamental relationships for motion of rock particles, as follows:

$$\rho\ddot{u} = \frac{\partial_{S_{ii}}}{\partial_x} + \frac{\partial_{S_{ij}}}{\partial_y} - 2S_{ij}\frac{\partial_w}{\partial_x} + (S_{ii} - S_{jj})\frac{\partial_w}{\partial_y} - \frac{\partial_{S_{ii}}}{\partial_x}e_{xx} - \frac{\partial_{S_{ij}}}{\partial_y}e_{yy} - \left(\frac{\partial_{S_{ii}}}{\partial_y} + \frac{\partial_{S_{ij}}}{\partial_x}\right)e_{xy} \quad (2)$$

$$\rho\ddot{v} = \frac{\partial_{S_{ij}}}{\partial_x} + \frac{\partial_{S_{jj}}}{\partial_y} - 2S_{ij}\frac{\partial_w}{\partial_y} + (S_{ii} - S_{jj})\frac{\partial_w}{\partial_x} - \frac{\partial_{S_{jj}}}{\partial_y}e_{yy} - \frac{\partial_{S_{ij}}}{\partial_y}e_{xx} - \left(\frac{\partial_{S_{jj}}}{\partial_x} + \frac{\partial_{S_{ij}}}{\partial_y}\right)e_{xy} \quad (3)$$

where $e_{xx} = \frac{\partial u}{\partial x}, e_{yy} = \frac{\partial v}{\partial y}, e_{xy} = \frac{\partial u}{\partial y} + \frac{\partial v}{\partial x}$, and $w = \frac{1}{2}\left(\frac{\partial v}{\partial x} - \frac{\partial u}{\partial y}\right)$

And S_{jj} is the primary pre-stress field (Pa); S_{ij} represents incremental stress (Pa) related to the wave. Moreover, u and v are incremental displacements (m) because of deformation, and ρ indicates the rock density (kg/m^3) [101]. The above formulation can be employed in forecasting seismic activity induced by CO_2 injection into the subsurface rocks.

3.3.2. Caprock Failure

Description

Caprock plays a crucial role in geosequestration projects. It must possess high density, integrity, and low permeability, enabling it to effectively trap injected CO_2 over an extended period [25]. Additionally, the caprock should exhibit remarkable strength under tension and compression conditions, withstanding the changing stress state during and after CO_2 injection [26]. These essential characteristics are pivotal in ensuring a secure CCS operation, necessitating thorough examination during project planning and CO_2 injection deployment [88].

Shear wave velocity data help in assessing the integrity of caprock formations in CCS projects. By measuring Vs in the CCS field, the mechanical stability and sealing capacity of the caprock can be continually examined or monitored. For instance, Blake et al. used Vs measurements and numerical simulation to evaluate the strength properties of caprock layers in Algeria [25]. Moreover, in a review paper, Gholami et al. described the methods of detecting CO_2 leakage by applying Vs data [102].

Rutqvist and Tsang developed a TOUGH-FLAC numerical code for CO_2 migration in an aquifer covered by a caprock [26]. They reported that caprock collapse (or instability) mainly occurs at the lower sections, since the effective mean stress remarkably declines in this segment. This lower section exhibits a pronounced susceptibility to hydraulic fracturing due to a limited pressure margin. This margin denotes the fluidic pressure level which caprock can withstand without experiencing notable failure. Such a margin is calculated to be merely 0.1 MPa after a decade of CO_2 injection [26].

Formulations

Generally, caprock mechanical stability can be evaluated through two approaches: analytical solutions and numerical simulations. In both cases, the Vs parameter can be utilized to calculate the elastic moduli of the caprock. Those elastic moduli are then included in analytical solutions or numerical models. The mechanical behavior of caprock can be specified using well-known rock failure criteria, such as Mohr–Coulomb, Hoek and Brown, modified lade, etc. [31]. To simulate the interplay of liquid carbon dioxide and caprock, the impact of pore pressure must be included throughout the entire analysis. Hence, an appropriate coupled fluid–rock analysis should be performed. The poroelasticity theory developed by Biot is capable of modeling such fluid–rock interactions [103]. The poroelastic

behavior is brought about by the pore fluid pressure in the pore spaces of rocks [104]. The fundamental relation in poroelasticity theory is [105,106]:

$$\acute{\sigma} = \sigma - \alpha p. \tag{4}$$

where $\acute{\sigma}$ shows effective stress (Pa); σ stands for total stress (Pa); p represents pore fluid pressure in caprock (Pa); α indicates the Biot's coefficient estimated through the underlying relationship [107]:

$$\alpha = 1 - \frac{K_{dry}}{K_m}. \tag{5}$$

where K_{dry} stands for dry caprock bulk modulus (Pa); K_m is the bulk modulus of the caprocks' minerals (Pa) [107]. K_{dry} is determined as [106]:

$$K_{dry} = \rho\left({V_p}^2 - \frac{4}{3}{V_s}^2\right) \tag{6}$$

where V_p (m/s) together with V_s (m/s) are velocities of compressional waves along with shear waves, respectively. Moreover, ρ indicates caprock density (kg/m^3).

It is widely acknowledged that any extent of CO_2 leakage through a damaged caprock presents a possible environmental issue [108]. Caprock leakage may occur as a result of caprock fracturing due to excessive pore pressure or because of the upward pressure applied by the stored CO_2 under the caprock. Several studies have addressed water/oil flow through rock fractures, and corresponding models have been established [109,110]. Despite this, there is a paucity of comprehensive research on the rheological characteristics of supercritical fluids within rocks' fractures. The study led by Yang et al. introduced a correlation between carbon dioxide transmissivity, fracture volume stress, and fracture pore pressure [37]. They introduced an empirical formula to describe the seepage of CO_2 gas through rock fractures under three-dimensional stress conditions, as follows:

$$T_{\mathrm{fg}} = 0.9416p^{-0.2788}\exp\{-0.0205[\sigma 1 - \alpha\ p] - 0.0053[0.6(\sigma_2 + \sigma_3) - 0.8\sigma_1]\} \tag{7}$$

where T_{fg} indicates seepage coefficient on fracture length (cm^3/atm.sec), σ_1 represents maximum stress acting in one direction (atm), σ_2 is the intermediate stress (atm), and σ_3 demonstrates minimum stress (atm) acting along the direction perpendicular to σ_1 and σ_2. The above formulae are applied for risk assessment of caprock failure in CCS projects.

3.3.3. Groundwater Contamination

Description

Until now, various investigations, both in the field and in laboratories, as well as numerical investigations, have been implemented to investigate the impacts of CCS on shallow groundwater aquifers [27]. Introducing CO_2 deep into the subsurface elevates fluid pressure within storage reservoirs. This heightened pressure has the potential to displace CO_2 towards upper aquifers through any existing leakage pathways [28]. The main leakage pathways through which CO_2 may migrate to aquifers include natural faults or discontinuities, active or abandoned wellbores, and the pore spaces within the caprock [38,82,111]. Figure 8 shows a schematic representation of those leakage pathways. Given that CO_2 is less dense than water, it can naturally ascend to shallower zones solely through buoyancy forces, even when a significant pressure gradient is not present. For instance, the density of supercritical CO_2 injected in the Ketzin CCS project, which is located near Berlin, was reported to be approximately 234.53 kg/m^3 [34]. In comparison, the density of fresh water is 1000 kg/m^3.

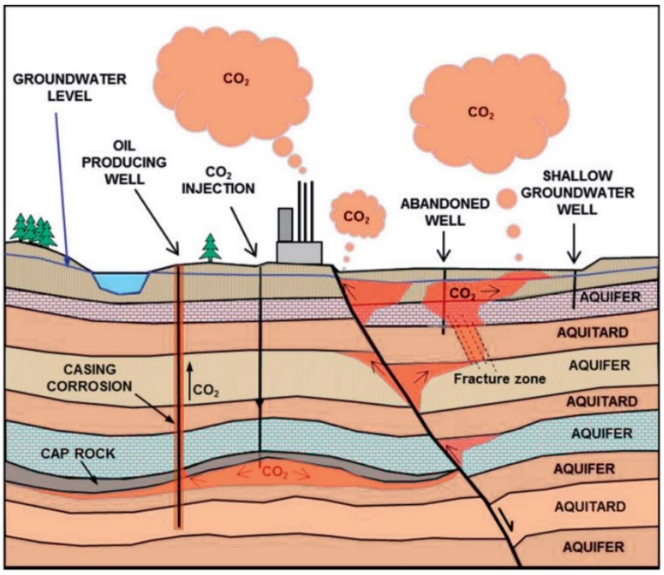

Figure 8. Schematic representation of CO_2 leakage pathways in CCS projects [112].

The carbon dioxide solubility in water tends to decrease with rising temperature. On the other hand, it increases with escalating pressure. This matter has been illustrated in Figure 9 [39]. If supercritical CO_2 leaks into the shallow water resources, the CO_2 will undergo a transition from a supercritical state to a gaseous state, during which it will partly or entirely dissolve into the existing water.

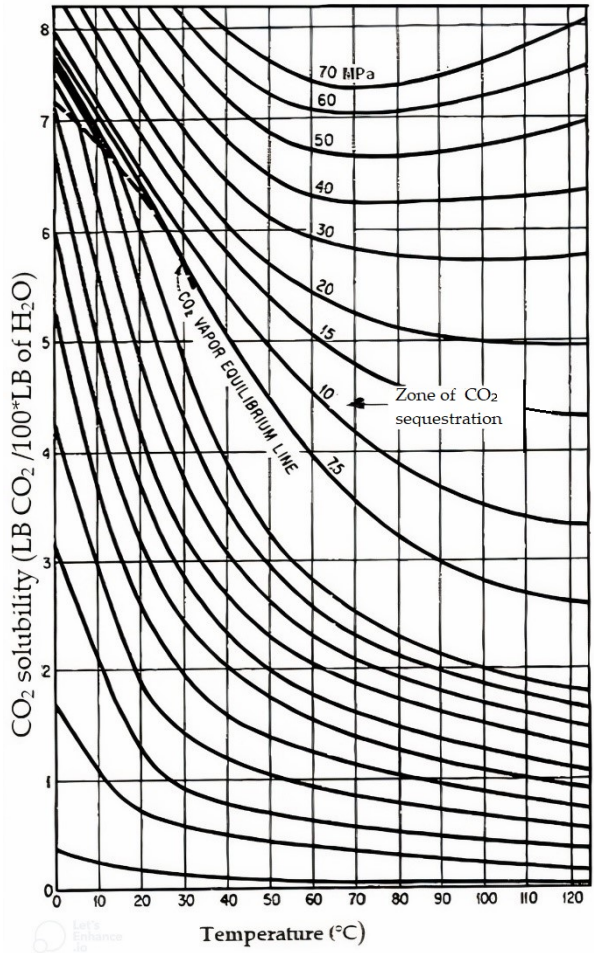

Figure 9. CO_2 solubility in water [39].

The dissolution of CO_2 into groundwater can lead to carbonic acid production, which causes a decline in pH as well as a rise in dissolved carbonate content. The chemical reaction process is [113] as follows:

$$CO_{2(g)} + H_2O = H_2CO_{3(aq)} \quad (8)$$

$$H_2CO_{3(aq)} = HCO_3^- + H^+ \quad (9)$$

The pH reduction and the rise in carbonate ligands have the potential to induce the release of naturally occurring metal (loid)s from aquifer rocks and sediments to the water [27,28]. Laboratory studies have noted reductions in pH and increased concentrations of metals, e.g., calcium (Ca), manganese (Mn), and iron (Fe), when various aquifer rocks were exposed to CO_2-charged waters [113,114]. Consequently, the quality of the water might be affected.

To achieve a safe, successful CCS operation, continuous monitoring of the sequestrated CO_2 is highly essential. Several geophysics-based techniques are applicable in monitoring CO_2 leakage into aquifers. Those techniques mainly used the electrical resistivity of rocks and their seismic velocity to inspect the variations in groundwater quality. Both electrical and seismic techniques are applicable in miscellaneous arrays, i.e., down-hole, surface, down-hole–surface, and cross-hole setups, to record subsurface data [115]. Selecting an efficient geophysical method for carbon dioxide leakage detection relies upon aquifer characteristics, like the anticipated largeness of the CO_2 storage area, the investigation depth, the presence of monitoring boreholes, the geological characteristics, and the extent of variations in physicochemical features resulting from CO_2 leakage. Electric methods are commonly employed for studying shallow groundwater aquifers [115]. In contrast, seismic and gravity-based methods find more frequent applications in monitoring CO_2 in deep subsurface areas.

Geophysical seismic measurements offer an appealing method for tracking CO_2 migration in subsurface areas. Because wave velocity and attenuation are responsive to alterations in storage formation pressure, time-lapse seismic techniques have frequently been employed to monitor the large-scale expansion of CO_2 plumes in rocks [34]. Xue et al. used the time-lapse induction technique to monitor CO_2 motion in the storage reservoir of the Nagaoka pilot site, Japan [40]. Moreover, CO_2 migration in the Nagaoka and Frio pilot sites was successfully mapped using cross-well seismic surveys [33,116]. While surface seismic observations at the field scale provide lower clarity compared to well logging and cross-well seismic methods, they allow for the monitoring of significantly broader regions [32–36,40,116].

Field-scale studies aside, laboratory-scale seismic investigations have also been conducted to monitor the CO_2 migration in rock samples. Kim et al. monitored CO_2 movements in water-saturated sandstone samples using a joint seismic and resistivity measurement approach [32]. In that study, seismic velocity tomography was successfully used to image CO_2 movement in rock specimens. Moreover, it was found that rock resistivity rises consistently during the injection operation, whereas seismic speed and wave amplitude experience significant declines as a consequence of CO_2 injection.

Formulations

In all the abovementioned seismic investigations, Gassmann's theory was chiefly applied in the calculation of the degree of CO_2 saturation in the rocks [34]. Distinguishing changes in fluid saturation involves comparing time-lapse records measured prior to and after the sequestration phase [32]. Gassmann's theory can be used to calculate the bulk modulus of the saturated rocks by using the following underlying equation [34,117]:

$$K_{sat} = K_{dry} + \frac{\left(1 - \frac{K_{dry}}{K_m}\right)^2}{\frac{\varphi}{K_{fluid}} + \frac{(1-\varphi)}{K_m} - \frac{K_{dry}}{K_m^2}} \quad (10)$$

where K_{sat} represents rocks' bulk modulus (Pa); φ indicates rock porosity; K_{fluid} represents pore fluid bulk modulus (Pa). After CO_2 injection, if CO_2 leaks into the aquifer, the density of the aquifer rock will change, since the mixture of CO_2 and water will have a different density. Consequently, for the aquifer rock, Gassmann's relationship can be adopted both prior to and after the CO_2 injection phase. Two parameters will change: K_{sat} and K_{fluid}. To calculate these two parameters, the following procedure can be utilized.

When the injected CO_2 leaks into the aquifer, the density of the mixed fluid can be estimated as [34]:

$$\rho_{fluid} = \rho_{water} S_{water} + (1 - S_{water}) \rho_{CO_2} \tag{11}$$

where ρ_{fluid} represents the density of the mixture of CO_2 and water (kg/m^3), ρ_{water} is water density (kg/m^3), S_{water} shows the water saturation degree in rocks (kg/m^3), and ρ_{co_2} depicts the CO_2 density (kg/m^3). Furthermore, the density of the porous rock containing the mixture of CO_2 and water can be calculated as [34]:

$$\rho_{sat} = \rho_{fluid} \varphi + (1 - \varphi) \rho_m \tag{12}$$

where ρ_{sat} represents the density of the porous rock (kg/m^3) and ρ_m stands for the density of the minerals of the rock (kg/m^3). Then, using the underlying relation, K_{sat} can be obtained as:

$$K_{sat} = \rho_{sat} \left({V_p}^2 - \frac{4}{3} {V_s}^2 \right) \tag{13}$$

Therefore, having the K_{sat}, the K_{fluid} can be calculated [106].

3.3.4. Fault Reactivation

Description

Faults and fractures play a crucial role in geomechanical investigations [118]. They represent potential pathways for fluid migration to aquifers [119,120]. CO_2 injection may lead to geomechanical repercussions, including the possibility of creating fractures and activating faults [29]. An elevation in pore pressure leads to an increase in the rock's permeability, since cracks and fractures open up, facilitating the escape of CO_2 from the storage zone [121].

So far, numerous studies have reported that extensive CO_2 injection might induce fault reactivation. For example, CO_2 injection in Decatur project, in the USA, reactivated certain minor faults [23]. Other examples include the Otway CCS site in Australia [85], the Teapot Dome CO_2-EOR site in USA [87], the Po River site in Italy [122], the Saint-Martin de Bossenay site in France [123], the In Salah site in Algeria [124], and the Snøhvit CCS site in Norway [91].

When faults undergo reactivation, structural changes take place in both the rock matrix and the pore fluid. Such changes will impact the rocks' elastic moduli, consequently resulting in measurable variations in seismic velocities, i.e., Vp and Vs [125]. A widely employed method for identifying reactivation faults is the passive monitoring of microseismic events. The detection of those events provides valuable insights into the origin as well as the fault triggering mechanism [90,126].

Successive seismic studies increasingly being carried out for monitoring CCS-originated subsurface changes, encompassing changes in stress state [127] and fluid composition [128]. Rivet et al. employed a time-lapse seismic approach to quantify seismic velocity fluctuations in a fault in shale formation. They linked the wave velocity variations to the pressurized pore fluids, which led to an increase in fault permeability [129]. In another study, Shadoan et al. conducted a time-lapse seismic study to analyze the fault reactivation mechanism [130]. During their experiments, a fault was monitored using the continuous active-source seismic monitoring (CASSM) technique [116,131]. This technique utilizes cross-well seismic sensors and receivers to tomographically assess minor variations in seis-

mic properties. This characteristic enables high-precision measurements of wave velocity and attenuation [130].

Badree and Alexander employed the petrophysical and geomechanical characteristics of a regional reservoir within the Cruse formation in Trinidad to evaluate the effect of injected carbon dioxide on fault reactivation [30]. Utilizing CMG-GEM software, they developed a model that simulated the formation response. The model incorporated the opening of a conductive fracture through tensile failure as pore pressure increased under total stress. Additionally, the migration of CO_2 along the fault was simulated using the Barton–Bandis failure criterion [30].

Formulations

A diverse spectrum of investigations has illustrated that stones, soils, and faults undergo strength degradation with increases in pore pressure [132–134]. In Figure 10, the Mohr diagram demonstrates the influence of escalating pore pressure on fault failure. In this figure, σ_1 and σ_3 are the most- and the least-confining stresses applied on a rock containing a fault. The τ parameter represents the shear stress applied to the surface of the fault. Furthermore, the angle between the fault surface and σ_1 is represented by θ, and σ_n represents the normal stress applied on the surface of the fault.

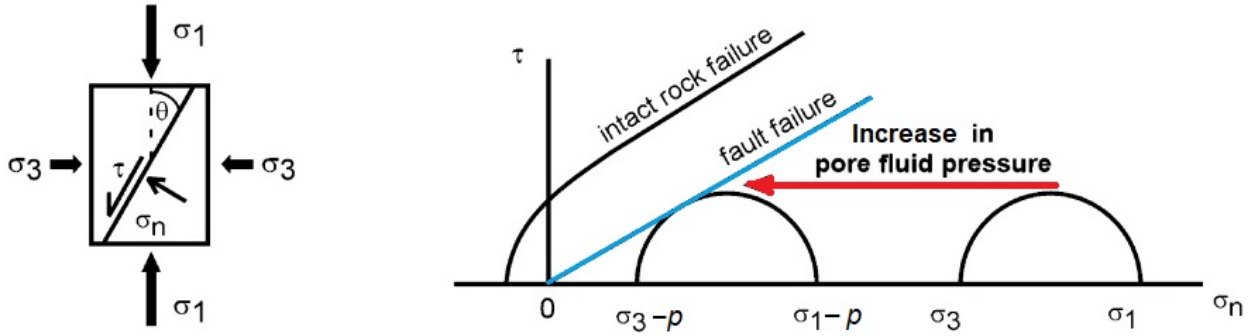

Figure 10. The impact of pore pressure increases on fault failure [21].

With an escalation in pore pressure in rock, there is a reduction in effective normal stress, causing the Mohr circle to approach the fault failure envelope. Such a matter has been illustrated in Figure 10. The failure envelope is typically determined through multiple frictional strength tests in laboratory settings [135,136]. The onset of fault failure is indicated when the Mohr circle intersects the fault failure envelope. Compared to an intact rock, faults undergo failure at lower shear stress levels. This is why the fault failure envelope lies on the right side of the intact rock failure envelope.

For the above case, the fault failure can be formulated as [39]:

$$\tau_{slp} = C_{fault} + (\sigma_n - \alpha p) tan\varphi_{fault}. \quad (14)$$

where τ_{slp} represents the fault slip shear stress (Pa); C_{fault} is the fault's cohesion (Pa); σ_n indicates normal stress (Pa); α stands for dimensionless Biot's coefficient; p represents pore pressure (Pa); φ_{fault} stands for fault friction angle (degree). For a cohesionless fault surface, the above equation can be simplified as follows [21]:

$$\tau_{slp} = (\sigma_n - \alpha p) tan\varphi_{fault}. \quad (15)$$

Hence, it can be said that fault reactivation (fault failure) takes place if the following is true:

$$tan\varphi_{fault} = \tau_{slp}/(\sigma_n - \alpha p). \quad (16)$$

The above equation can be utilized to define the dimensionless factor of fault slip tendency, as follows:

$$T_s = \tau_{slp}/(\sigma_n - \alpha p). \quad (17)$$

where T_s is the dimensionless fault tendency [21].

In deep rock layers, some parameters, such as pore pressure and local stress regime, play significant roles in rock geomechanical behavior [137]. Except for these two factors, fault orientation is also of paramount importance in fault reactivation analysis [21]. To determine the fault orientations, 2D or 3D seismic measurements are conducted. If such fault orientations are obtained using the depth-converted 3D seismic measurements, then T_s is computed for each point of the fault through Equation (17).

A typical illustration of fault slip tendency modeled on the basis of 3D seismic data is presented in Figure 11. In this figure, the contours of T_s on the fault surface have been shown for a depth interval from 0 m to 3500 m [21]. Utilizing the recorded seismic profiles helps in ensuring accurate geomechanical modeling, enabling the incorporation of factors such as fault surface curvature in fault slip assessment. Therefore, for fault stability analyses, it is advised to record 3D seismic data, and incorporate them in analytical or numerical modelling.

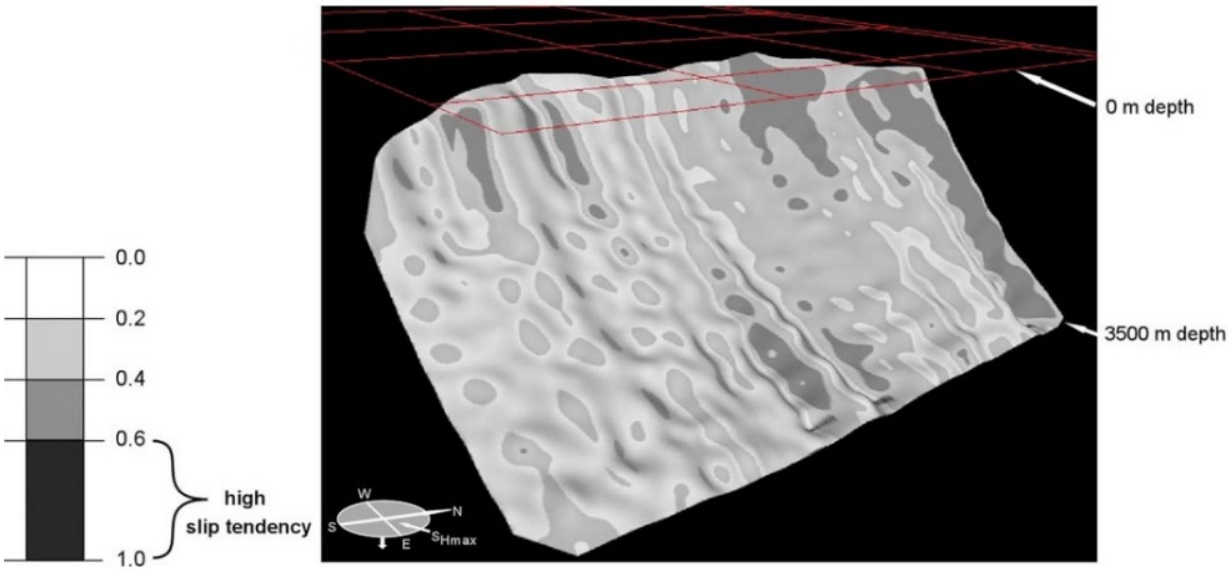

Figure 11. Contour map of slip tendency of a fault studied by [21].

CO_2 sequestration initiatives require the high-precision calculation of sustainable fluid pressures that avoid inducing fracturing or triggering faults, which could potentially result in the escape of CO_2. Hence, it is of the utmost significance to ascertain the optimal injection pressure for CO_2 to assess the consequential impacts on fault reactivation. The maximum pore pressure to avoid fault reactivation may be evaluated by incrementally raising the pore fluid pressure level in Equation (17) [21]. The upper limit for CO_2 injection pressure can be considered as the pore pressure at which a fault slips. Thus, the CO_2 injection pressures must be maintained under this maximum limit to prevent any failure-related issues.

Equation (17) clearly shows that the fault failure potential strongly relies upon the pore fluid pressure and Biot's coefficient. Thus, it may be said that fault reactivation analysis due to the CO_2 injection is a hydromechanical problem. Such a hydromechanical coupling analysis has been used by different researchers to predict fault reactivation [138–140].

3.3.5. Reservoir Deformation

Description

Reservoir deformation is a concern in the context of CCS projects, especially since substantial CO_2 injections can bring about two crucial issues.

Firstly, CO_2 injection can bring about pore pressure increases within storage rocks. Such elevated pore pressures may induce stress changes and impact the reservoir integrity, potentially leading to deformation. As a matter of fact, when pore pressure changes, the

local stress regime is disturbed [141], which can result in the compaction or expansion of the reservoir rock. Such a deformation may affect the stability and porosity of the rock, influencing the storage capacity and the ability to contain injected CO_2 [31].

Secondly, as a consequence of CO_2 injection, the reservoir may exhibit geomechanical responses, such as subsidence or uplift. Subsidence can impact surface infrastructure and ecosystems [142,143], while uplift may disturb the natural equilibrium of the subsurface.

Formulations

Monitoring and modeling techniques are employed to predict the geomechanical behavior of the reservoir, helping to minimize risks associated with reservoir deformation [144,145]. The Vs parameter belongs to the key monitoring factors used in geomechanical assessments of CCS projects. By measuring the speed at which shear waves propagate through the subsurface, geoscientists can estimate the elastic moduli and other characteristics of subsurface rocks. Equations (18)–(22) are commonly used to calculate those properties [31,118]:

$$\nu = \frac{\frac{1}{2} - \left(V_s/V_p\right)^2}{1 - \left(V_s/V_p\right)^2} \tag{18}$$

$$E = \rho \frac{V_p^2(1+\nu)(1-2\nu)}{(1-\nu)} \tag{19}$$

$$G = \rho V_s^2 \tag{20}$$

$$\lambda = \rho\left(V_p^2 - 2V_s^2\right) \tag{21}$$

$$k = \frac{1}{K} \tag{22}$$

In the above equations, ν stands for a rock's Poisson's ratio, and E represents Young's modulus (Pa). Furthermore, ρ indicates rock bulk density (kg/m^3); G represents rock shear modulus (Pa); λ is Lame's constant (Pa); k is rock compressibility (Pa^{-1}).

Long-term Vs monitoring allows for the detection of changes in subsurface conditions [146]. In fact, anomalies in shear wave velocity can indicate alterations in the mechanical properties of a rock, thereby providing insights into potential deformation or stress changes. By incorporating Vs data into Equations (18)–(22), engineers can improve the accuracy of the geomechanical models and enhance the predictions related to reservoir deformation. Therefore, a continuous monitoring of shear wave velocity can serve as an early-warning system for potential geomechanical issues. Changes in shear wave velocity may precede observable deformation, providing an opportunity to take preventive measures or adjust injection parameters.

4. Discussion

The main applications of Vs parameters in geomechanics were elaborated upon in the earlier sections. Moreover, the study revealed how Vs data can be efficiently incorporated into CCS risk assessments. The ongoing utilization of Vs data in geo-related projects is expected to be more extensive as new measurement sensors and instruments are capable of recording the acoustic wave velocities with higher accuracy. Shear wave velocity is increasingly applied in rocks characterization, not only on Earth but also on remote planets [147–149].

Risk assessment is an indispensable part of any geo-related project [150,151]. The successful implementation of CCS initiatives relies heavily on the accurate assessment of geological formations to guarantee secure and efficient CO_2 sequestration. The utilization of shear wave velocity data in seismic surveys enhances the accuracy of subsurface characterization.

By incorporating Vs information into seismic models, researchers and operators can more precisely delineate geological features, identify potential pathways for CO_2

migration, and assess the spatial distribution of stress and strain within the storage reservoir. In other words, Vs data can be utilized to estimate the bulk modulus, Poisson's ratio, and Young's modulus, and to share modules of the subsurface rocks volume by using Equations (13) and (18)–(20). When these parameters are estimated, they can be imported into 3D numerical simulations that can be performed in commercial programs such as Abaqus and FLAC3D. Then, by running numerical models, the stress redistribution and mechanical deformations (strains) of the reservoir rocks can be calculated. Moreover, the Vs data can be applied to determine the fault orientations on CCS sites. If the fault orientations are ascertained, then the fault sleep tendency can be calculated through Equation (17). This approach enables geomechanics and engineers to classify the local faults based on their sleep tendency. Hence, the susceptible faults for CO_2 migration can be detected.

When supercritical CO_2 is injected into a target reservoir, the pore pressure in the reservoir increases. Consequently, as the injection process proceeds, CO_2 may escape from the reservoir. Since injected CO_2 is lighter than water, it migrates towards the upper strata and the ground surface. So far, several studies that have been performed in laboratory settings or in the field have shown that CO_2 leakage can occur through fault fractures or abandoned wells [82,111]. The possible mechanisms of CO_2 migration can be categorized into fast and slow mechanism types. In the fast mechanism, CO_2 migrates through the abandoned wells in the area, local faults, and rocks' discontinuities. On the contrary, in the slow mechanism, CO_2 mainly leaks through the gradual dissolution of the caprock [82,111].

Furthermore, the sensitivity of shear wave velocity to fluid saturation levels is a critical aspect of CCS risk assessment [152,153]. Changes in fluid content within storage formations can significantly alter Vs, serving as an indicator of potential leakage or CO_2 migration. In other words, risks including induced seismicity, caprock failure, water contamination, fault reactivation, and reservoir deformation are directly dependent on pore pressure, which in turn affects Vs magnitude in rocks. Thus, it can be deduced that the assessment of CCS-induced risks is a coupled hydromechanical analysis. This matter is evident, with Equations (4), (7) and (10)–(17) reflecting the role of pore pressure and Biot's coefficient in risk analysis formulations. According to this point, the authors highlight that a precise measurement of poroelastic parameters is of paramount significance in CCS risk assessment. Hence, providing high-precision field instruments and laboratory apparatuses for Vs measurement is highly recommended.

Despite the evident significance of shear wave velocity in CCS risk assessment, some challenges remain in its application. Variability in geological formations, complex interactions between different rock types, and uncertainties in Vs measurements contribute to the complexity of accurately predicting subsurface conditions [154–158]. Future research efforts should focus on refining measurement techniques, developing predictive models that account for geological heterogeneity, and conducting field-scale experiments to validate the findings of laboratory studies.

The joint monitoring approach, involving the integration of multiple geophysical methods such as geoelectric and seismic surveys, have frequently been effective in minimizing monitoring uncertainties and enhancing accuracy [145]. In many cases, supplementary measurements like well-logging data, borehole fluid analysis, and CO_2 flow characteristics may be utilized to refine and validate geophysical data. Beyond electrical and seismic measurements, precise gravity monitoring may also serve as another valuable tool for detecting variations in density and pressure resulting from CO_2 injection. This enables the tracking of CO_2 migration or potential leakage in the subsurface [83].

The classic techniques for Vs measurement, e.g., laboratory-scale experiments and wellbore surveys, have long been the gold standard in geoengineering studies. While providing accurate results, they are often time-consuming, labor-intensive, and expensive, thereby making them less feasible for large-scale assessments [159]. Geophysical methods, including seismic refraction [160], surface wave analysis [161,162], and seismic tomography [163] offer cost-effective and energy-efficient alternatives to traditional laboratory

testing and borehole measurements. These methods have demonstrated their practical applications in characterizing Vs profiles and capturing variations in complex geological settings [164]. However, they also have limitations related to data availability, sensitivity to site conditions, and the need for controlled seismic sources.

5. Conclusions

This comprehensive review underscores the pivotal role of shear wave velocity in the assessment of the critical risks induced by CCS operations. Vs emerges as a versatile parameter, contributing significantly to various geomechanical analyses, including induced seismicity, caprock stability, groundwater contamination, fault reactivation, and reservoir deformation. The multifaceted nature of CCS technologies necessitates the ongoing monitoring of CO_2 plume migration. Vs data provide valuable insights into subsurface conditions, acting as an early-warning system for potential geomechanical and environmental issues.

As CCS technologies continue to evolve, the significance of shear wave velocity remains paramount. Its applications extend beyond being a mere monitoring tool, positioning Vs as a key parameter in optimizing injection pressures, predicting seismic events, and preventing the contamination of potable shallow groundwater resources. The journey toward sustainable carbon storage requires a holistic approach, encompassing technological innovation, rigorous scientific inquiry, and collaborative efforts across disciplines. With shear wave velocity as a guiding metric, the future of CCS technology holds promise for a safer, more efficient, and environmentally responsible approach to mitigating carbon emissions.

The geomechanical interaction between injected CO_2 and porous rocks can be numerically modeled through poroelasticity theory. Since the majority (nearly 99%) of CCS projects are operated in saline aquifers and exhausted hydrocarbon reservoirs, any prior geomechanical data obtained from exploratory boreholes, laboratory measurements, etc., are very useful in calibrating the Vs values recorded during geophysical seismic surveys. As an example, once the static elastic moduli of underground rocks are measured through exploratory boreholes, the dynamic elastic moduli calculated from the seismic surveys can be accurately calibrated.

The generation of 3D geomechanical models provides an exceptional visual approach for assessing the influence of CO_2 sequestration on subsurface rocks. To accurately create such models, the quantity and spatial distribution of in situ stresses must be determined through standard tests, such as the leak-off test. Moreover, the native pore pressure must be precisely estimated before liquid CO_2 injection. In addition, the distribution and orientation of local faults must be carefully studied and quantified. Access to these three data categories will help geomechanics and engineers in generating 3D models that are capable of accurately predicting CCS-induced risks.

Furthermore, continued research which deepens our understanding of the underlying physics of Vs behavior in various geological settings will contribute to the development of improved models and Vs prediction methods. Incorporating geological knowledge and geophysical insights into predictive models will enhance their interpretability and practical applicability in CCS scenarios.

In conclusion, shear wave velocity emerges as a valuable tool in CCS risk assessment, providing critical insights into the mechanical and fluid-related aspects of storage formations. Its integration into comprehensive risk evaluation frameworks enhances the reliability of CCS projects, guaranteeing the long-lasting viability and safety of carbon capture and sequestration plans. Overall, the future of shear wave velocity applications in CCS projects is optimistic, with potential advancements contributing to more effective risk assessments, improved monitoring, and enhanced strategies for mitigating environmental impacts.

Author Contributions: Conceptualization, formal analysis, methodology, writing—review and editing, writing—original draft preparation, and investigation, M.K. and D.K.; supervision, validation, project administration, D.K. All authors have read and agreed to the published version of the manuscript.

Funding: The project was supported by the AGH University of Krakow, subsidy 16.16.190.779.

Data Availability Statement: All used data are accessible in the article.

Acknowledgments: The authors wish to extend their appreciation to Mohammad Zamani Ahmad Mahmoudi, currently pursuing a PhD at AGH University in Krakow, for his valuable assistance throughout the conduction of this study.

Conflicts of Interest: The authors of this paper declare no conflicts of interest.

References

1. Shafiee, A.; Azadi, A. Shear-wave velocity characteristics of geological units throughout Tehran City, Iran. *J. Asian Earth Sci.* **2007**, *29*, 105–115. [CrossRef]
2. S-Wave Motion. Available online: https://www.iris.edu/hq/inclass/animation/swave_motion (accessed on 22 January 2024).
3. L'Heureux, J.S.; Long, M. Relationship between shear-wave velocity and geotechnical parameters for Norwegian clays. *J. Geotech. Geoenviron. Eng.* **2017**, *143*, 04017013. [CrossRef]
4. Knez, D.; Rajaoalison, H. Discrepancy between Measured Dynamic Poroelastic Parameters and Predicted Values from Wyllie's Equation for Water-Saturated Istebna Sandstone. *Acta Geophys.* **2021**, *69*, 673–680. [CrossRef]
5. Sundararajan, N.; Seshunarayana, T. Shear wave velocities in the estimation of earthquake hazard over alluvium in a seismically active region. *J. Geol. Soc. India* **2018**, *92*, 259–264. [CrossRef]
6. Jamiolkowski, M. Role of geophysical testing in geotechnical site characterization. *Soils Rocks* **2012**, *35*, 117–137. [CrossRef]
7. Anbazhagan, P.; Sitharam, T.G. Site characterization and site response studies using shear wave velocity. *J. Seismol. Earthq. Eng.* **2008**, *10*, 53–67.
8. Li, X.Y.; Zhang, Y.G. Seismic reservoir characterization: How can multicomponent data help? *J. Geophys. Eng.* **2011**, *8*, 123. [CrossRef]
9. Crampin, S.; McGonigle, R.; Bamford, D. Estimating crack parameters from observations of P-wave velocity anisotropy. *Geophysics* **1980**, *45*, 345–360. [CrossRef]
10. Hedtmann, N.; Alber, M. Investigation of water-permeability and ultrasonic wave velocities of German Malm aquifer rocks for hydro-geothermal energy. In Proceedings of the ISRM European Rock Mechanics Symposium—EUROCK 2017, Ostrava, Czech Republic, 20–22 June 2017.
11. Sharifi-Mood, M.; Olsen, M.J.; Gillins, D.T.; Mahalingam, R. Performance-based, seismically-induced landslide hazard mapping of Western Oregon. *Soil Dyn. Earthq. Eng.* **2017**, *103*, 38–54. [CrossRef]
12. Peuchen, J.; De Ruijter, M.R.; Hospers, B.; Assen, R.L. Shear wave velocity integrated in offshore geotechnical practice. In Proceedings of the SUT Offshore Site Investigation and Geotechnics, London, UK, 26–28 November 2002.
13. Hosseini, K.; Matthews, K.J.; Sigloch, K.; Shephard, G.E.; Domeier, M.; Tsekhmistrenko, M. SubMachine: Web-based tools for exploring seismic tomography and other models of Earth's deep interior. *Geochem. Geophys. Geosyst.* **2018**, *19*, 1464–1483. [CrossRef]
14. Ikeda, T.; Tsuji, T. Robust subsurface monitoring using a continuous and controlled seismic source. *Energy Procedia* **2017**, *114*, 3956–3960. [CrossRef]
15. Roy, P.; Mohanty, A.K.; Misra, M. Prospects of Carbon Capture, Utilization and Storage for Mitigating Climate Change. *Environ. Sci. Adv.* **2023**, *2*, 409–423. [CrossRef]
16. Global Climate Highlights 2023. Available online: https://climate.copernicus.eu/global-climate-highlights-2023#:~:text=2023%20marks%20the%20first%20time,than%202%C2%B0C%20warmer (accessed on 20 January 2024).
17. Eggleston, H.S.; Buendia, L.; Miwa, K.; Ngara, T.; Tanabe, K. *Guidelines for National Greenhouse Gas Inventories*; IGES: Kanagawa, Japan, 2006.
18. Nordhaus, W.D. An Optimal Transition Path for Controlling Greenhouse Gases. *Science* **1992**, *258*, 1315–1319. [CrossRef] [PubMed]
19. Graphics. Available online: https://www.ipcc.ch/sr15/graphics/ (accessed on 10 May 2023).
20. Aminu, M.D.; Nabavi, S.A.; Rochelle, C.A.; Manovic, V. A Review of Developments in Carbon Dioxide Storage. *Appl. Energy* **2017**, *208*, 1389–1419. [CrossRef]
21. Streit, J.E.; Hillis, R.R. Estimating fault stability and sustainable fluid pressures for underground storage of CO_2 in porous rock. *Energy* **2004**, *29*, 1445–1456. [CrossRef]
22. Nicol, A.; Carne, R.; Gerstenberger, M.; Christophersen, A. Induced Seismicity and Its Implications for CO_2 Storage Risk. *Energy Procedia* **2011**, *4*, 3699–3706. [CrossRef]
23. White, J.A.; Foxall, W. Assessing Induced Seismicity Risk at CO_2 Storage Projects: Recent Progress and Remaining Challenges. *Int. J. Greenh. Gas Control* **2016**, *49*, 413–424. [CrossRef]
24. Rathnaweera, T.D.; Wu, W.; Ji, Y.; Gamage, R.P. Understanding Injection-Induced Seismicity in Enhanced Geothermal Systems: From the Coupled Thermo-Hydro-Mechanical-Chemical Process to Anthropogenic Earthquake Prediction. *Earth-Sci. Rev.* **2020**, *205*, 103182. [CrossRef]
25. Blake, O.O.; Faulkner, D.R.; Worden, R.H.; Armitage, P.J.; Espie, A.A. Effect of thermal shock on the permeability and seismic wave velocity of the caprock and reservoir during CO_2 injection. *Int. J. Greenh. Gas Control.* **2022**, *118*, 103691. [CrossRef]

26. Rutqvist, J.; Tsang, C.F. A Study of Caprock Hydromechanical Changes Associated with CO_2-Injection into a Brine Formation. *Environ. Geol.* **2002**, *42*, 296–305. [CrossRef]
27. Zheng, L.; Apps, J.A.; Zhang, Y.; Xu, T.; Birkholzer, J.T. On Mobilization of Lead and Arsenic in Groundwater in Response to CO_2 Leakage from Deep Geological Storage. *Chem. Geol.* **2009**, *268*, 281–297. [CrossRef]
28. Apps, J.A.; Zheng, L.; Zhang, Y.; Xu, T.; Birkholzer, J.T. Evaluation of potential changes in groundwater quality in response to CO_2 leakage from deep geologic storage. *Transp. Porous Media* **2010**, *82*, 215–246. [CrossRef]
29. Rutqvist, J.; Rinaldi, A.P.; Cappa, F.; Moridis, G.J. Modeling of fault reactivation and induced seismicity during hydraulic fracturing of shale-gas reservoirs. *J. Pet. Sci. Eng.* **2013**, *107*, 31–44. [CrossRef]
30. Badree, A.; Alexander, D. Fault Reactivation and CO_2 Migration in Carbon Storage in a Saline Aquifer. *Int. J. Clim. Change Impacts Responses* **2021**, *14*, 129. [CrossRef]
31. Fjaer, E.; Holt, R.M.; Horsrud, P.; Raaen, A.M. *Petroleum Related Rock Mechanics*; Elsevier: Amsterdam, The Netherlands, 2008.
32. Kim, J.; Matsuoka, T.; Xue, Z. Monitoring and detecting CO_2 injected into water-saturated sandstone with joint seismic and resistivity measurements. *Explor. Geophys.* **2011**, *42*, 58. [CrossRef]
33. Saito, H.; Nobuoka, D.; Azuma, H.; Tanase, D.; Xue, Z. Time-lapse crosswell seismic tomography for monitoring the CO_2 injected into an onshore aquifer, Nagaoka, Japan. In Proceedings of the 8th SEGJ International Symposium, Society of Exploration Geophysicists of Japan, Tokyo, Japan, 26–28 November 2006; pp. 1–4. [CrossRef]
34. Ivanova, A.; Kashubin, A.; Juhojuntti, N.; Kummerow, J.; Henninges, J.; Juhlin, C.; Lüth, S.; Ivandic, M. Monitoring and volumetric estimation of injected CO_2 using 4D seismic, petrophysical data, core measurements, and well logging: A case study at Ketzin, Germany. *Geophys. Prospect.* **2012**, *60*, 957–973. [CrossRef]
35. Chadwick, R.A.; Noy, D.; Arts, R.; Eiken, O. Latest time-lapse seismic data from Sleipner yield new insights into CO_2 plume development. *Energy Procedia* **2009**, *1*, 2103–2110. [CrossRef]
36. Ajo-Franklin, J.B.; Peterson, J.; Doetsch, J.; Daley, T.M. High-resolution characterization of a CO_2 plume using crosswell seismic tomography: Cranfield, MS, USA. *Int. J. Greenh. Gas Control* **2013**, *18*, 497–509. [CrossRef]
37. Yang, D.; Zhao, Y.; Hu, Y. The Constitutive Law of Gas Seepage in Rock Fractures Undergoing Three-Dimensional Stress. *Transp. Porous Media* **2006**, *63*, 463–472. [CrossRef]
38. Wildenborg, T.; Leijnse, T.; Kreft, E.; Nepveu, M.; Obdam, A. Long-term Safety Assessment of CO2 Storage: The Scenario Approach. In Proceedings of the 7th International Conference on Greenhouse Gas Control Technologies, Vancouver, Canada, 5–September 2004; Elsevier: Amsterdam, The Netherlands, 2005. [CrossRef]
39. Shukla, R.; Ranjith, P.; Haque, A.; Choi, X. A Review of Studies on CO_2 Sequestration and Caprock Integrity. *Fuel* **2010**, *89*, 2651–2664. [CrossRef]
40. Xue, Z.; Tanase, D.; Watanabe, J. Estimation of CO_2 saturation from time-lapse CO_2 well logging in an onshore aquifer, Nagaoka, Japan. *Explor. Geophys.* **2006**, *37*, 19. [CrossRef]
41. Boore, D.M.; Joyner, W.B.; Fumal, T.E. Equations for estimating horizontal response spectra and peak acceleration from western North American earthquakes: A summary of recent work. *Seismol. Res. Lett.* **1997**, *68*, 128–153. [CrossRef]
42. Dong, Y.; Lu, N. Dependencies of shear wave velocity and shear modulus of soil on saturation. *J. Eng. Mech.* **2016**, *142*, 04016083. [CrossRef]
43. Thitimakorn, T.; Channoo, S. Shear wave velocity of soils and NEHRP site classification map of Chiang Rai City, Northern Thailand. *Electron. J. Geotech. Eng.* **2012**, *17*, 2891–2904.
44. Pitilakis, K.; Riga, E.; Anastasiadis, A. Design spectra and amplification factors for Eurocode 8. *Bull. Earthq. Eng.* **2012**, *10*, 1377–1400. [CrossRef]
45. Idriss, I.M.; Boulanger, R.W. *Soil Liquefaction during Earthquakes*; Earthquake Engineering Research Institute: Oakland, CA, USA, 2008.
46. Rodriguez-Marek, A.; Bray, J.D.; Abrahamson, N.A. A geotechnical seismic site response evaluation procedure. In Proceedings of (Vol. 12). 2000. Available online: https://www.iitk.ac.in/nicee/wcee/article/1590.pdf (accessed on 26 February 2024).
47. Uma Maheswari, R.; Boominathan, A.; Dodagoudar, G.R. Use of surface waves in statistical correlations of shear wave velocity and penetration resistance of Chennai soils. *Geotech. Geol. Eng.* **2010**, *28*, 119–137. [CrossRef]
48. Oh, T.M.; Bang, E.S.; Cho, G.C.; Park, E.S. Estimation of undrained shear strength for saturated clay using shear wave velocity. *Mar. Georesour. Geotechnol.* **2017**, *35*, 236–244. [CrossRef]
49. Baxter, C.D.; Bradshaw, A.S.; Green, R.A.; Wang, J.H. Correlation between cyclic resistance and shear-wave velocity for providence silts. *J. Geotech. Geoenviron. Eng.* **2008**, *134*, 37–46. [CrossRef]
50. Yunmin, C.; Han, K.; Ren-peng, C. Correlation of shear wave velocity with liquefaction resistance based on laboratory tests. *Soil Dyn. Earthq. Eng.* **2005**, *25*, 461–469. [CrossRef]
51. Josh, M.; Esteban, L.; Delle Piane, C.; Sarout, J.; Dewhurst, D.N.; Clennell, M.B. Laboratory characterisation of shale properties. *J. Pet. Sci. Eng.* **2012**, *88*, 107–124. [CrossRef]
52. Wang, Y.; Mooney, W.D.; Yuan, X.; Okaya, N. Crustal structure of the northeastern Tibetan Plateau from the southern Tarim Basin to the Sichuan Basin, China. *Tectonophysics* **2013**, *584*, 191–208. [CrossRef]
53. Kováčik, J.; Emmer, Š. Correlation between shear wave velocity and porosity in porous solids and rocks. *J. Powder Technol.* **2013**, *2013*, 643167. [CrossRef]
54. Korneev, V. Slow waves in fractures filled with viscous fluid. *Geophysics* **2008**, *73*, N1–N7. [CrossRef]

55. Azhar, A.S.B.; Latiff, A.H.A.; Lim, L.H.; Gödeke, S.H. Groundwater investigation of a coastal aquifer in Brunei Darussalam using seismic refraction. *Environ. Earth Sci.* **2019**, *78*, 1–17. [CrossRef]
56. Jarvis, K.D.; Knight, R.J. Aquifer heterogeneity from SH-wave seismic impedance inversion. *Geophysics* **2002**, *67*, 1548–1557. [CrossRef]
57. Alhumimidi, M.S. An integrated approach for identification of seawater intrusion in coastal region: A case study of northwestern Saudi Arabia. *J. King Saud Univ.-Sci.* **2020**, *32*, 3187–3194. [CrossRef]
58. Mourad, M.; Tsuji, T.; Ikeda, T.; Ishitsuka, K.; Senna, S.; Ide, K. Mapping aquifer storage properties using s-wave velocity and insar-derived surface displacement in the Kumamoto area, Southwest Japan. *Remote Sens.* **2021**, *13*, 4391. [CrossRef]
59. Sayers, C.M. Elastic wave velocities in a granitic geothermal reservoir. *Geophys. Prospect.* **2022**, *71*, 114–124. [CrossRef]
60. Lou, M.; Rial, J.A. Characterization of geothermal reservoir crack patterns using shear-wave splitting. *Geophysics* **1997**, *62*, 487–494. [CrossRef]
61. Wawerzinek, B.; Buness, H.; von Hartmann, H.; Tanner, D.C. S-wave experiments for the exploration of a deep geothermal carbonate reservoir in the German Molasse Basin. *Geotherm. Energy* **2021**, *9*, 1–21. [CrossRef]
62. Mendrinos, D.; Karytsas, C.; Karytsas, S.; Poletto, F.; Farina, B.; Barison, E. Correlations of Seismic Velocities and Elastic Moduli with Temperature in Superhot and Enhanced Geothermal Systems. *Clean Technol.* **2022**, *4*, 440–457. [CrossRef]
63. Del Gaudio, V.; Muscillo, S.; Wasowski, J. What we can learn about slope response to earthquakes from ambient noise analysis: An overview. *Eng. Geol.* **2014**, *182*, 182–200. [CrossRef]
64. Qureshi, M.U.; Yamada, S.; Towhata, I. A simplified technique for slope stability assessment based on in-situ S-wave velocity measurement. In *Earthquake-Induced Landslides: Proceedings of the International Symposium on Earthquake-Induced Landslides, Kiryu, Japan, 2012*; Springer: Berlin/Heidelberg, Germany, 2013; pp. 871–881. [CrossRef]
65. Chen, Y.; Irfan, M.; Uchimura, T.; Wu, Y.; Yu, F. Development of elastic wave velocity threshold for rainfall-induced landslide prediction and early warning. *Landslides* **2019**, *16*, 955–968. [CrossRef]
66. Feng, Z.Y.; Lu, Y.R.; Shen, Z.R. A numerical simulation of seismic signals of coseismic landslides. *Eng. Geol.* **2021**, *289*, 106191. [CrossRef]
67. Nadim, F.; Kvalstad, T.J. Risk assessment and management for offshore geohazards. In Proceedings of the ISGSR2007 First International Symposium on Geotechnical Safety & Risk, Shanghai, China, 18–19 November 2007; pp. 18–19.
68. Ten Brink, U.S.; Lee, H.J.; Geist, E.L.; Twichell, D. Assessment of tsunami hazard to the US East Coast using relationships between submarine landslides and earthquakes. *Mar. Geol.* **2009**, *264*, 65–73. [CrossRef]
69. Zhao, M.; Gao, Z.; Wang, P.; Du, X. Response spectrum method for seismic analysis of monopile offshore wind turbine. *Soil Dyn. Earthq. Eng.* **2020**, *136*, 106212. [CrossRef]
70. Huijer, C.; Harajli, M.; Sadek, S. Upgrading the seismic hazard of Lebanon in light of the recent discovery of the offshore thrust fault system. *Leban. Sci. J.* **2011**, *12*, 67.
71. Mainprice, D.; Tommasi, A.; Couvy, H.; Cordier, P.; Frost, D.J. Pressure sensitivity of olivine slip systems and seismic anisotropy of Earth's upper mantle. *Nature* **2005**, *433*, 731–733. [CrossRef]
72. Gao, W.; Grand, S.P.; Baldridge, W.S.; Wilson, D.; West, M.; Ni, J.F.; Aster, R. Upper mantle convection beneath the central Rio Grande rift imaged by P and S wave tomography. *J. Geophys. Res. Solid Earth* **2004**, *109*. [CrossRef]
73. Zhang, Z.; Yao, H.; Yang, Y. Shear wave velocity structure of the crust and upper mantle in Southeastern Tibet and its geodynamic implications. *Sci. China Earth Sci.* **2020**, *63*, 1278–1293. [CrossRef]
74. Butler, R.; Tsuboi, S. Antipodal seismic reflections upon shear wave velocity structures within Earth's inner core. *Phys. Earth Planet. Inter.* **2021**, *321*, 106802. [CrossRef]
75. Bachu, S. Sequestration of CO_2 in Geological Media: Criteria and Approach for Site Selection in Response to Climate Change. *Energy Convers. Manag.* **2000**, *41*, 953–970. [CrossRef]
76. SCCS. Available online: https://www.sccs.org.uk/resources/downloads (accessed on 11 February 2021).
77. SCCS. Available online: https://www.sccs.org.uk/resources/global-ccs-map (accessed on 11 February 2021).
78. Mahajan, O.P. CO_2 surface area of coals: The Z-year paradox. *Carbon* **1991**, *29*, 735–742. [CrossRef]
79. Krooss, B.V.; Van Bergen, F.; Gensterblum, Y.; Siemons, N.; Pagnier, H.J.M.; David, P. High-Pressure Methane and Carbon Dioxide Adsorption on Dry and Moisture-Equilibrated Pennsylvanian Coals. *Int. J. Coal Geol.* **2002**, *51*, 69–92. [CrossRef]
80. Zevenhoven, R.; Fagerlund, J.; Songok, J.K. CO_2 Mineral Sequestration: Developments Toward Large-Scale Application. *Greenh. Gases Sci. Technol.* **2011**, *1*, 48–57. [CrossRef]
81. Rohmer, J.; Pluymakers, A.; Renard, F. Mechano-Chemical Interactions in Sedimentary Rocks in the Context of CO_2 Storage: Weak Acid, Weak Effects? *Earth Sci. Rev.* **2016**, *157*, 86–110. [CrossRef]
82. Lemieux, J.M. The Potential Impact of Underground Geological Storage of Carbon Dioxide in Deep Saline Aquifers on Shallow Groundwater Resources. *Hydrogeol. J.* **2011**, *19*, 757–778. [CrossRef]
83. Alnes, H.; Eiken, O.; Nooner, S.; Sasagawa, G.; Stenvold, T.; Zumberge, M. Results from Sleipner gravity monitoring: Updated density and temperature distribution of the CO_2 plume. *Energy Procedia* **2011**, *4*, 5504–5511. [CrossRef]
84. Daley, T.M.; Sharma, S.; Dzunic, A.; Urosevic, M.; Kepic, A.; Sherlock, D. *Borehole Seismic Monitoring at Otway Using the Naylor-1 Instrument String*; Lawrence Berkeley National Lab. (LBNL): Berkeley, CA, USA, 2009. [CrossRef]
85. Vidal-Gilbert, S.; Tenthorey, E.; Dewhurst, D.; Ennis-King, J.; Van Ruth, P.; Hillis, R. Geomechanical analysis of the Naylor Field, Otway Basin, Australia: Implications for CO_2 injection and storage. *Int. J. Greenh. Gas Control* **2010**, *4*, 827–839. [CrossRef]

86. Stork, A.L.; Nixon, C.G.; Hawkes, C.D.; Birnie, C.; White, D.J.; Schmitt, D.R.; Roberts, B. Is CO_2 Injection at Aquistore Aseismic? A Combined Seismological and Geomechanical Study of Early Injection Operations. *Int. J. Greenh. Gas Control* **2018**, *75*, 107–124. [CrossRef]
87. Chiaramonte, L.; Zoback, M.D.; Friedmann, J.; Stamp, V. Seal integrity and feasibility of CO_2 sequestration in the Teapot Dome EOR pilot: Geomechanical site characterization. *Environ. Geol.* **2008**, *54*, 1667–1675. [CrossRef]
88. Watson, M.N.; Gibson-Poole, C.M. Reservoir Selection for Optimised Geological Injection and Storage of Carbon Dioxide: A Combined Geochemical and Stratigraphic Perspective. In *The Fourth Annual Conference on Carbon Capture and Storage*; National Energy Technology Laboratory, US Department of Energy: Alexandria, VA, USA, 2005; pp. 2–5.
89. Verdon, J.P.; Kendall, J.M.; White, D.J.; Angus, D.A.; Fisher, Q.J.; Urbancic, T. Passive Seismic Monitoring of Carbon Dioxide Storage at Weyburn. *Lead. Edge* **2010**, *29*, 200–206. [CrossRef]
90. Goertz-Allmann, B.P.; Kühn, D.; Oye, V.; Bohloli, B.; Aker, E. Combining microseismic and geomechanical observations to interpret storage integrity at the In Salah CCS site. *Geophys. J. Int.* **2014**, *198*, 447–461. [CrossRef]
91. Chiaramonte, L.; Johnson, S.; White, J.A. Preliminary geomechanical analysis of CO_2 injection at Snøhvit, Norway. In Proceedings of the 45th U.S. Rock Mechanics/Geomechanics Symposium, San Francisco, CA, USA, 26–29 June 2011.
92. CSIRO. Available online: https://www.csiro.au/en/research/natural-environment/natural-resources/otway-project (accessed on 18 October 2019).
93. CSIRO. Available online: https://www.geos.ed.ac.uk/sccs/project-info/1901 (accessed on 11 October 2016).
94. Global CCS Institute. Available online: https://www.globalccsinstitute.com/news-media/insights/china-continues-to-advance-ccus-in-2023-learning-by-doing-after-launch-of-first-integrated-megaton-project-underscore-momentum/ (accessed on 20 July 2023).
95. Gan, W.; Frohlich, C. Gas Injection May Have Triggered Earthquakes in the Cogdell Oil Field, Texas. *Proc. Natl. Acad. Sci. USA* **2013**, *110*, 18786–18791. [CrossRef] [PubMed]
96. Hovorka, S.D.; Meckel, T.A.; Trevino, R.H. Monitoring a Large-Volume Injection at Cranfield, Mississippi—Project Design and Recommendations. *Int. J. Greenh. Gas Control* **2013**, *18*, 345–360. [CrossRef]
97. Verdon, J.P.; Stork, A.L. Carbon Capture and Storage, Geomechanics and Induced Seismic Activity. *J. Rock Mech. Geotech. Eng.* **2016**, *8*, 928–935. [CrossRef]
98. Payre, X.; Maisons, C.; Marblé, A.; Thibeau, S. Analysis of the Passive Seismic Monitoring Performance at the Rousse CO_2 Storage Demonstration Pilot. *Energy Procedia* **2014**, *63*, 4339–4357. [CrossRef]
99. Myer, L.R.; Daley, T.M. Elements of a Best Practices Approach to Induced Seismicity in Geologic Storage. *Energy Procedia* **2011**, *4*, 3707–3713. [CrossRef]
100. Kissling, C.; Cherry, J.T. Excitation of Earthquakes by Underground Explosions. *Trans. Am. Geophys. Union* **1970**, *51*, 353.
101. Kisslinger, C. A Review of Theories of Mechanisms of Induced Seismicity. *Eng. Geol.* **1976**, *10*, 85–98. [CrossRef]
102. Gholami, R.; Raza, A.; Iglauer, S. Leakage risk assessment of a CO_2 storage site: A review. *Earth-Sci. Rev.* **2021**, *223*, 103849. [CrossRef]
103. Biot, M.A. General Theory of three-dimensional consolidation. *J. Appl. Phys.* **1941**, *12*, 155–164. [CrossRef]
104. Khalilidermani, M.; Knez, D. A Survey on the Shortcomings of the Current Rate of Penetration Predictive Models in Petroleum Engineering. *Energies* **2023**, *16*, 4289. [CrossRef]
105. Zamani, M.A.M.; Knez, D. Experimental Investigation on the Relationship between Biot's Coefficient and Hydrostatic Stress for Enhanced Oil Recovery Projects. *Energies* **2023**, *16*, 4999. [CrossRef]
106. Knez, D.; Khalilidermani, M.; Zamani, M.A.M. Water Influence on the Determination of the Rock Matrix Bulk Modulus in Reservoir Engineering and Rock-Fluid Coupling Projects. *Energies* **2023**, *16*, 1769. [CrossRef]
107. Knez, D.; Zamani, M.A.M. Empirical Formula for Dynamic Biot Coefficient of Sandstone Samples from South-West of Poland. *Energies* **2021**, *14*, 5514. [CrossRef]
108. Saripalli, P.; McGrail, P. Semi-Analytical Approaches to Modeling Deep Well Injection of CO_2 for Geological Sequestration. *Energy Convers. Manag.* **2002**, *43*, 185–198. [CrossRef]
109. Hildenbrand, A.; Schlömer, S.; Krooss, B.M.; Littke, R. Gas Breakthrough Experiments on Pelitic Rocks: Comparative Study with N_2, CO_2, and CH_4. *Geofluids* **2004**, *4*, 61–80. [CrossRef]
110. Liu, L.; Suto, Y.; Bignall, G.; Yamasaki, N.; Hashida, T. CO_2 Injection to Granite and Sandstone in Experimental Rock/Hot Water Systems. *Energy Convers. Manag.* **2003**, *44*, 1399–1410. [CrossRef]
111. Lions, J.; Devau, N.; de Lary, L.; Dupraz, S.; Parmentier, M.; Gombert, P.; Dictor, M.C. Potential Impacts of Leakage from CO_2 Geological Storage on Geochemical Processes Controlling Fresh Groundwater Quality: A Review. *Int. J. Greenh. Gas Control* **2014**, *22*, 165–175. [CrossRef]
112. Brydie, J.R.; Perkins, E.H.; Fisher, D.; Girard, M.; Valencia, M.; Olson, M.; Rattray, T. The Development of a Leak Remediation Technology for Potential Non-Wellbore Related Leaks from CO_2 Storage Sites. *Energy Procedia* **2014**, *63*, 4601–4611. [CrossRef]
113. Varadharajan, C.; Tinnacher, R.M.; Trautz, R.C.; Zheng, L.; Dafflon, B.; Wu, Y.; Reagan, M.T.; Birkholzer, J.T.; Carey, J.W. A Review of Studies Examining the Potential for Groundwater Contamination from CO_2 Sequestration. In *Geological Carbon Storage: Subsurface Seals and Caprock Integrity*; Wiley: Hoboken, NJ, USA, 2018; pp. 305–326. [CrossRef]
114. Little, M.G.; Jackson, R.B. Potential impacts of leakage from deep CO_2 geosequestration on overlying freshwater aquifers. *Environ. Sci. Technol.* **2010**, *44*, 9225–9232. [CrossRef] [PubMed]

115. Khalilidermani, M.; Knez, D.; Zamani, M.A.M. Empirical Correlations between the Hydraulic Properties Obtained from the Geoelectrical Methods and Water Well Data of Arak Aquifer. *Energies.* **2021**, *14*, 5415. [CrossRef]
116. Daley, T.M.; Myer, L.R.; Peterson, J.E.; Majer, E.L.; Hoversten, G.M. Time-lapse crosswell seismic and VSP monitoring of injected CO_2 in a brine aquifer. *Environ. Geol.* **2007**, *54*, 1657–1665. [CrossRef]
117. Gassmann, F. Über die Elastizität poröser Medien. *Vierteljahrsschr. Naturforschenden Ges. Zur.* **1951**, *96*, 1–23.
118. Zoback, M.D. *Reservoir Geomechanics*; Cambridge University Press: Cambridge, UK, 2010.
119. Oldenburg, C.M.; Bryant, S.L.; Nicot, J.-P. Certification framework based on effective trapping for geologic carbon sequestration. *Int. J. Greenh. Gas Control* **2009**, *3*, 444–457. [CrossRef]
120. Song, J.; Zhang, D. Comprehensive review of caprock-sealing mechanisms for geologic carbon sequestration. *Environ. Sci. Technol.* **2013**, *47*, 9–22. [CrossRef] [PubMed]
121. Rutqvist, J. Fractured rock stress–permeability relationships from in situ data and effects of temperature and chemical–mechanical couplings. In *Crustal Permeability*; Wiley: Hoboken, NJ, USA, 2012; pp. 65–82. [CrossRef]
122. Ferronato, M.; Gambolati, G.; Janna, C.; Teatini, P. Geomechanical issues of anthropogenic CO_2 sequestration in exploited gas fields. *Energy Convers. Manag.* **2010**, *51*, 1918–1928. [CrossRef]
123. Vidal-Gilbert, S.; Nauroy, J.F.; Brosse, E. 3D geomechanical modelling for CO_2 geologic storage in the Dogger carbonates of the Paris Basin. *Int. J. Greenh. Gas Control* **2009**, *3*, 288–299. [CrossRef]
124. Rutqvist, J.; Vasco, D.W.; Myer, L. Coupled reservoir-geomechanical analysis of CO_2 injection and ground deformations at In Salah, Algeria. *Int. J. Greenh. Gas Control* **2010**, *4*, 225–230. [CrossRef]
125. Mavko, G.; Mukerji, T.; Dvorkin, J. *The Rock Physics Handbook*; Cambridge University Press: Cambridge, UK, 2020.
126. Goertz-Allmann, B.; Gibbons, S.; Oye, V.; Bauer, R.; Will, R. Characterization of induced seismicity patterns derived from internal structure in event clusters. *J. Geophys. Res. Solid Earth* **2017**, *122*, 3875–3894. [CrossRef]
127. Herwanger, J.V.; Mohamed, F.R.; Newman, R.; Vejbæk, O. Time-lapse seismic data-calibrated geomechanical model reveals hydraulic fracture re-orientation. In Proceedings of the 2013 SEG Annual Meeting, Houston, TX, USA, 22–27 September 2013.
128. Blazevic, L.A.; Bodet, L.; Pasquet, S.; Linde, N.; Jougnot, D.; Longuevergne, L. Time-lapse seismic and electrical monitoring of the vadose zone during a controlled infiltration experiment at the ploemeur hydrological observatory, France. *Water* **2020**, *12*, 1230. [CrossRef]
129. Rivet, D.; De Barros, L.; Guglielmi, Y.; Cappa, F.; Castilla, R.; Henry, P. Seismic Velocity Changes Associated with Aseismic Deformations of a Fault Stimulated by Fluid Injection. *Geophys. Res. Lett.* **2016**, *43*, 9563–9572. [CrossRef]
130. Shadoan, T.A.; Ajo-Franklin, J.B.; Guglielmi, Y.; Wood, T.; Robertson, M.; Cook, P.; Soom, F.; Daley, T.M.; Hopp, C.; Tribaldos, V.R.; et al. Active-Source Seismic Imaging of Fault Re-activation and Leakage: An Injection Experiment at the Mt Terri Rock Laboratory, Switzerland. *Geophys. Res. Lett.* **2023**, *50*, e2023GL104080. [CrossRef]
131. Ajo-Franklin, J.; Daley, T.; Butler-Veytia, B.; Peterson, J.; Wu, Y.; Kelly, B.; Hubbard, S. Multi-level Continuous Active Source Seismic Monitoring (ML-CASSM): Mapping Shallow Hydrofracture Evolution at a TCE Contaminated Site. In Proceedings of the 2011 SEG Annual Meeting, San Antonio, TX, USA, 18–23 September 2011.
132. Blanpied, M.L.; Lockner, D.A.; Byerlee, J.D. An Earthquake Mechanism Based on Rapid Sealing of Faults. *Nature* **1992**, *358*, 574–576. [CrossRef]
133. Handin, J.; Hager Jr, R.V.; Friedman, M.; Feather, J.N. Experimental Deformation of Sedimentary Rocks under Confining Pressure: Pore Pressure Tests. *Bull. Am. Assoc. Petrol. Geol.* **1963**, *47*, 717–755.
134. Zamani, M.A.M.; Knez, D. A new mechanical-hydrodynamic safety factor index for sand production prediction. *Energies* **2021**, *14*, 3130. [CrossRef]
135. Jaeger, J.C.; Cook, N.G.W. *Fundamentals of Rock Mechanics*; Methuen & Co. Ltd.: London, UK, 1969.
136. Byerlee, J. *Friction of Rocks*; Birkhäuser: Basel, Switzerland, 1987; pp. 615–626. [CrossRef]
137. Khalilidermani, M.; Knez, D. A Survey of Application of Mechanical Specific Energy in Petroleum and Space Drilling. *Energies* **2022**, *15*, 3162. [CrossRef]
138. Chang, K.W.; Segall, P. Injection-Induced Seismicity on Basement Faults Including Poroelastic Stressing. *J. Geophys. Res. Solid Earth* **2016**, *121*, 2708–2726. [CrossRef]
139. Cao, W.; Shi, J.-Q.; Durucan, S.; Korre, A. Evaluation of Shear Slip Stress Transfer Mechanism for Induced Micro-seismicity at In Salah CO_2 Storage Site. *Int. J. Greenh. Gas Control* **2021**, *107*, 103302. [CrossRef]
140. Kroll, K.A.; Buscheck, T.A.; White, J.A.; Richards-Dinger, K.B. Testing the Efficacy of Active Pressure Management as a Tool to Mitigate Induced Seismicity. *Int. J. Greenh. Gas Control* **2020**, *94*, 102894. [CrossRef]
141. Knez, D.; Zamani, O.A.M. Up-to-Date Status of Geoscience in the Field of Natural Hydrogen with Consideration of Petroleum Issues. *Energies* **2023**, *16*, 6580. [CrossRef]
142. Knez, D.; Rajaoalison, H. Land Subsidence Assessment for Wind Turbine Location in the South-Western Part of Madagascar. *Energies* **2022**, *15*, 4878. [CrossRef]
143. Rajaoalison, H.; Knez, D.; Zamani, M.A.M. A Multidisciplinary Approach to Evaluate the Environmental Impacts of Hydrocarbon Production in Khuzestan Province, Iran. *Energies* **2022**, *15*, 8656. [CrossRef]
144. Arts, R.; Eiken, O.; Chadwick, A.; Zweigel, P.; van der Meer, L.; Zinszner, B. Monitoring of CO_2 Injected at Sleipner Using Time-Lapse Seismic Data. *Energy* **2004**, *29*, 1383–1392. [CrossRef]

145. Kazemeini, S.H.; Juhlin, C.; Fomel, S. Monitoring CO_2 Response on Surface Seismic Data: A Rock Physics and Seismic Modeling Feasibility Study at the CO_2 Sequestration Site, Ketzin, Germany. *J. Appl. Geophys.* **2010**, *71*, 109–124. [CrossRef]
146. Kazemeini, H.; Juhlin, C.; Zinck-Jørgensen, K.; Norden, B. Application of the Continuous Wavelet Transform on Seismic Data for Mapping of Channel Deposits and Gas Detection at the CO_2SINK Site, Ketzin, Germany. *Geophys. Prospect.* **2009**, *57*, 111–123. [CrossRef]
147. Knez, D.; Zamani, M.A.M. A Review of the Geomechanics Aspects in Space Exploration. *Energies* **2021**, *14*, 7522. [CrossRef]
148. Knez, D.; Khalilidermani, M. A Review of Different Aspects of Off-Earth Drilling. *Energies* **2021**, *14*, 7351. [CrossRef]
149. Khalilidermani, M.; Knez, D. A Survey on Extraterrestrial Habitation Structures with a Focus on Energy-Saving 3D Printing Techniques. *Appl. Sci.* **2023**, *13*, 12913. [CrossRef]
150. Wurdemann, H.; Moeller, F.; Kuhn, M.; Heidug, W.; Christensen, N.P.; Borm, G.; Schilling, F.R.; CO_2SINK Group. CO_2SINK—From Site Characterisation and Risk Assessment to Monitoring and Verification: One Year of Operational Experience with the Field Laboratory for CO_2 Storage at Ketzin, Germany. *Int. J. Greenh. Gas Control* **2010**, *4*, 938–951. [CrossRef]
151. Mostafaei, K.; Mahmoudi, M.Z.A.; Knez, D. Risk Management Prediction of Mining and Industrial Projects by Support Vector Machine. *Resour. Policy* **2022**, *78*, 102819. [CrossRef]
152. Sakurai, S.; Ramakrishnan, T.S.; Boyd, A.; Mueller, N.; Hovorka, S. Monitoring Saturation Changes for CO_2 Sequestration: Petrophysical Support of the Frio Brine Pilot Experiment. In Proceedings of the 46th Annual Logging Symposium Transactions, Society of Petrophysicists and Well Log Analysts, New Orleans, LA, USA, 1 December 2006.
153. Meadows, M. Time-Lapse Seismic Modeling and Inversion of CO_2 Saturation for Storage and Enhanced Oil Recovery. *Lead. Edge* **2008**, *27*, 506–516. [CrossRef]
154. Scherbaum, F.; Hinzen, K.G.; Ohrnberger, M. Determination of shallow shear wave velocity profiles in the Cologne, Germany area using ambient vibrations. *Geophys. J. Int.* **2003**, *152*, 597–612. [CrossRef]
155. Valcke, S.L.A.; Casey, M.; Lloyd, G.E.; Kendall, J.M.; Fisher, Q.J. Lattice preferred orientation and seismic anisotropy in sedimentary rocks. *Geophys. J. Int.* **2006**, *166*, 652–666. [CrossRef]
156. Durante, M.G.; Karamitros, D.; Di Sarno, L.; Sica, S.; Taylor, C.A.; Mylonakis, G.; Simonelli, A.L. Characterisation of shear wave velocity profiles of non-uniform bi-layer soil deposits: Analytical evaluation and experimental validation. *Soil Dyn. Earthq. Eng.* **2015**, *75*, 44–54. [CrossRef]
157. Miah, M.I. Improved prediction of shear wave velocity for clastic sedimentary rocks using hybrid model with core data. *J. Rock Mech. Geotech. Eng.* **2021**, *13*, 1466–1477. [CrossRef]
158. Toro, G.R. Uncertainty in shear-wave velocity profiles. *J. Seismol.* **2022**, *26*, 713–730. [CrossRef]
159. Khalilidermani, M.; Knez, D. Comparing Artificial Intelligence Algorithms with Empirical Correlations in Shear Wave Velocity Prediction. *Appl. Sci.* **2023**, *13*, 13126. [CrossRef]
160. Sarkar, R.; Kolathayar, S.; Drukpa, D.; Choki, K.; Rai, S.; Tshering, S.T.; Yuden, K. Near-surface seismic refraction tomography and MASW for site characterization in Phuentsholing, Bhutan Himalaya. *SN Appl. Sci.* **2021**, *3*, 394. [CrossRef]
161. Nazarian, S. In Situ Determination of Elastic Moduli of Soil Deposits and Pavement Systems by Spectral-Analysis-of-Surface-Waves Method (Shear Velocity, Propagation, Liquefaction, Non-Destructive, Earthquake). Ph.D. Thesis, The University of Texas at Austin, Austin, TX, USA, 1984.
162. Boore, D.M. Determining subsurface shear-wave velocities: A review. In Proceedings of the Third International Symposium on the Effects of Surface Geology on Seismic Motion, Grenoble, France, 30 August–1 September 2006; pp. 67–85.
163. Li, Y.; Wu, Q.; Pan, J.; Sun, L. S-wave velocity structure of northeastern China from joint inversion of Rayleigh wave phase and group velocities. *Geophys. J. Int.* **2012**, *190*, 105–115. [CrossRef]
164. Pugin, A.J.M.; Pullan, S.E.; Hunter, J.A.; Oldenborger, G.A. Hydrogeological prospecting using P-and S-wave landstreamer seismic reflection methods. *Near Surf. Geophys.* **2009**, *7*, 315–328. [CrossRef]